Check for updates

CANCER

Single-nucleotide variant profiling in liquid biopsy with RECO-Cas

Chong Guo[1,2], Shuo Zhang[1,2], Ramachandra Yerramsetti[1], Jiongyu Zhang[1], Xin Guan[1,2], Rui Yang[1,2], Chengyu Hou[1,2], Minjie Pei[1,2], Kurt T. Schalper[1,2], Xingye Liu[1,2], Ziyue Li[1,2], Lorrie Perpetua[3], Wenqi Gan[4], Omar Ibrahim[5], Rachael A. Clark[6], Changchun Liu[1]*

Copyright © 2026 The Authors, some rights reserved; exclusive licensee American Association for the Advancement of Science. No claim to original U.S. Government Works. Distributed under a Creative Commons Attribution NonCommercial License 4.0 (CC BY-NC).

Mutation detection of cell-free DNA (cfDNA) through liquid biopsy is essential for precision oncology, resistance profiling, and informed clinical decision-making. However, its clinical application has remained limited by the lack of simple, rapid, accurate, and cost-effective detection approaches. Here, we report a recombined DNA construct–activated Cas12a (RECO-Cas) assay for profiling cfDNA mutations. The RECO-Cas assay uses a recombined DNA construct generated from Argonaute-nicked mutant DNA and an artificial DNA activator to selectively trigger CRISPR-Cas12a, enabling 0.01% variant allele frequency sensitivity and single-nucleotide resolution. Using the assay, we detect *KRAS*, *EGFR*, and *PIK3CA* point mutations in cfDNA from clinical plasma samples, demonstrating high sensitivity (90.48%) and excellent specificity (100%). We also apply it to successfully classify and identify *KRAS* missense variants. RECO-Cas provides a simple, rapid, and affordable solution that is compatible with a compact, wirelessly powered point-of-care diagnostic platform incorporating smartphone-based fluorescence detection. This assay enables highly sensitive and specific detection of low-frequency mutations, facilitating early cancer diagnosis and supporting the development of personalized treatment strategies.

INTRODUCTION

Blood-based liquid biopsy is a minimally invasive approach for early cancer detection, tissue-of-origin classification, and treatment monitoring. By analyzing circulating tumor biomarkers—such as circulating tumor DNA (ctDNA), circulating tumor cells (CTCs), and extracellular vesicles—from blood samples, this approach provides real-time insights into tumor progression and treatment response (*1*–*5*). Despite challenges such as low biomarker abundance and limited sensitivity, ongoing technological advances continue to expand its clinical utility, particularly for early detection and for tracking the heterogeneity and evolutionary dynamics of cancers (*6*–*8*).

Circulating cell-free DNA (cfDNA) comprises fragmented DNA released into the bloodstream during apoptosis and necrosis of both normal and tumor cells (*9*, *10*). In patients with cancer, a subset known as ctDNA originates from malignant cells and harbors tumor-specific genetic and epigenetic alterations, including point mutations (e.g., $KRAS^{G12D}$ and $PIK3CA^{E545K}$), insertions and deletions, copy number changes, and structural variants (*11*–*13*). Because ctDNA reflects the tumor's genomic profile, its analysis enables noninvasive cancer characterization. ctDNA detection in liquid biopsy has demonstrated clinical utility in early cancer detection, real-time monitoring of tumor burden and treatment response, identification of actionable mutations (e.g., $EGFR^{L858R}$), and detection of minimal residual disease or recurrence (*14*, *15*). Unlike tissue biopsies, which are limited by sampling constraints, cfDNA analysis captures tumor heterogeneity and allows longitudinal assessment from small blood volumes.

Despite widespread adoption, cfDNA mutation analysis still faces substantial technical and practical barriers. In early-stage or low-tumor-burden disease, ctDNA often represents <1% of total cfDNA, pushing existing assays to their sensitivity limits (*16*–*19*). To overcome this, most assay workflows incorporate one or more of the following approaches: allele-specific polymerase chain reaction (PCR) (*20*), blocker-based or clamp-mediated amplicon enrichment (*21*), molecular barcodes (*22*), and hybrid-capture sequencing (*23*), which increase cost, turnaround time, and procedural complexity. For instance, broad-coverage next-generation sequencing (NGS) demands multistep library preparation, high DNA input, and intensive bioinformatics, whereas droplet digital PCR (ddPCR) delivers subpercent sensitivity only for predefined loci and scales poorly (*6*, *24*, *25*). In addition, extensive sample handling, specialized instrumentation, and susceptibility to preanalytical variables (e.g., cfDNA fragmentation, genomic DNA carryover, and degradation) restrict routine or decentralized use. These limitations underscore the need for a streamlined, enrichment-free platform capable of quantifying rare mutations directly from microliter-scale cfDNA with high sensitivity and specificity, using minimal instrumentation, to enable simple and affordable point-of-care (POC) diagnostic applications in resource-limited settings.

Programmable endonucleases such as CRISPR-Cas9/12a and Argonaute proteins (e.g., *TtAgo*) have shown potential utility in cfDNA mutation detection because of their sequence-specific cleavage activity. Cas9-based assays [e.g., dCas9-based minor-allele enrichment (*26*) and CRISPR-CPPC (*27*)] couple DNA cleavage with PCR or specifically capture mutant cfDNA to amplify mutant allele fractions, enabling sensitive detection of known variants. However, because Cas12a's trans-cleavage activity is nonspecific, it is unsuitable for direct mutation enrichment; moreover, its mismatch tolerance hampers single-nucleotide variant (SNV) discrimination, leading to false positives in the direct detection of mutant sequences (*28*). Conversely, Argonaute proteins cleave single-base mismatches with high fidelity and has been applied to DNA mutation detection by depleting wild-type

[1]Department of Biomedical Engineering, University of Connecticut Health Center, Farmington, CT 06030, USA. [2]Department of Biomedical Engineering, University of Connecticut, Storrs, CT 06269, USA. [3]Research Tissue Repository, University of Connecticut Health Center, Farmington, CT 06030, USA. [4]Department of Public Health Sciences, University of Connecticut Health Center, Farmington, CT 06030, USA. [5]Department of Medicine, Division of Pulmonary, Critical Care, and Sleep Medicine, University of Connecticut Health Center, Farmington, CT 06030, USA. [6]Department of Dermatology, Brigham and Women's Hospital, Harvard Medical School, Boston, MA 02115, USA.
*Corresponding author. Email: chaliu@uchc.edu

Downloaded from https://www.science.org on May 23, 2026

alleles to enrich rare variants, as in A-Star (*29*) and NAVIGATER (*30*). Yet, because Argonaute proteins lack inherent signal amplification, it still requires advanced instruments—such as ddPCR systems or NGS platforms—for mutant sequence detection.

Here, we report a recombined DNA construct–activated Cas12a (RECO-Cas) assay to profile cfDNA mutations, enabling simple, sensitive, and accurate SNV detection in liquid biopsy. RECO-Cas integrates recombinase polymerase amplification (RPA), *TtAgo*-mediated precise cleavage of mutant DNA, and CRISPR-enabled signal amplification. To streamline the workflow, we combine target DNA amplification with *TtAgo*-mediated recognition and cleavage in a single-tube format. In the assay, the mutant allele is first amplified and cleaved, while wild-type DNA remains intact. The resulting nicked mutant allele then hybridizes with the Cas12a/CRISPR RNA (crRNA)/single-stranded DNA (ssDNA) activator complex, specifically triggering Cas12a trans-cleavage activity and amplifying the detection signal. RECO-Cas achieves sensitivity down to 0.01% variant allele frequency (VAF). Using the assay, we simultaneously detect multiple mutations in cfDNA extracted from a single patient plasma sample because of its sequence-specific signal amplification, enabling SNV profiling for early cancer detection. We further incorporate RECO-Cas into a compact, wirelessly powered diagnostic platform and detect fluorescence signals using an artificial intelligence (AI)–powered smartphone, highlighting its potential for minimally instrumented POC testing. In summary, the RECO-Cas assay enables simple, rapid, enrichment-free detection of low-frequency cfDNA mutations, providing a robust and scalable solution for liquid biopsy, well suited to resource-limited settings.

RESULTS

Overall RECO-Cas workflow

The RECO-Cas assay combines cfDNA isothermal amplification, *TtAgo* sequence–specific cleavage, and CRISPR-Cas12a–enabled signal amplification detection. It mainly consists of two steps: (a) a one-pot RPA-*TtAgo* reaction, in which a multiphase reaction system couples RPA amplification with *TtAgo* cleavage to enable selective nicking of mutant cfDNA amplicons while leaving wild-type amplicons intact [Fig. 1A (a)], and (b) mutant-specific CRISPR detection using a recombined DNA construct of nicked mutant DNA and artificial ssDNA (termed "ssDNA activator"). In the presence of mutant cfDNA, the Cas12a-crRNA complex recognizes the recombined DNA construct, inducing Cas12a conformational activation and subsequent trans-cleavage, thereby amplifying the fluorescence signal of mutant cfDNA. In contrast, even in the presence of ssDNA activators, intact wild-type DNA remains double-stranded and fails to unwind for crRNA recognition, thereby preventing Cas12a activation and subsequent reporter cleavage [Fig. 1A (ii)]. Although preanalytical steps such as plasma separation and DNA extraction require minimal bench-top instrumentation, we streamlined the downstream SNV detection workflow to make cfDNA analysis more compatible with POC early cancer detection (Fig. 1B). To eliminate the need for expensive instrumentation, we integrated the assay into a compact, wirelessly powered diagnostic platform, where fluorescence signals are detected using an AI-powered smartphone, enabling POC diagnostics in resource-limited settings.

The RECO-Cas assay offers key technical advantages for SNV detection. First, it provides highly specific mutation detection by leveraging the highly selective cleavage activity of the *TtAgo*-guide DNA complex (*30*). By strategically introducing a single-base mismatch within the guide DNA, we enabled *TtAgo* to distinguish and nick DNA mutants with single-nucleotide resolution, even within a complex background of wild-type or unrelated sequences. This strategy selectively introduces nicks into mutant DNA. In addition, 3′-terminal phosphorylation of the guide DNA further improves the specificity of cleavage and inhibits DNA extension by the DNA polymerase in the RPA reaction solution. Second, RECO-Cas achieves high detection sensitivity [low limit of detection (LoD)] with minimal background through two key mechanisms: (i) The absence of a nick causes wild-type DNA to retain its duplex structure, preventing spontaneous unwinding of the crRNA recognition region and thereby blocking crRNA binding and downstream activation, and (ii) Cas12a tolerates short ssDNA activators, and its trans-cleavage activity is not triggered (*31*). Only in the presence of nicked mutant DNA can the ssDNA activator form a recombined DNA structure and specifically bind the Cas12a-crRNA complex, triggering Cas12a DNase activity for fluorescence signal amplification. Owing to these unique features, RECO-Cas is capable of accurate profiling of multiple cancer mutations while achieving highly precise SNV detection.

Validation and optimization of the RECO-Cas assay

The RECO-Cas assay uses recombined *TtAgo*-nicked mutant DNA together with an ssDNA activator to specifically activate CRISPR-Cas12a for cfDNA mutation detection. To evaluate the design rationale, we first tested synthetic nucleotides corresponding to $KRAS^{G12D}$ and *wild-type KRAS* ($KRAS^{WT}$). When ssDNA was used as input, RECO-Cas failed to discriminate between mutant and wild-type alleles, as end-point fluorescence signals showed no substantial difference (fig. S1). By contrast, double-stranded DNA achieved robust, allele-specific detection of the mutant sequence. Mechanistically, RECO-Cas relies on spontaneous unwinding of the mutant allele at the crRNA recognition region near the nick, thereby facilitating crRNA hybridization. We further hypothesized that using dual guide DNAs targeting both strands of the mutant sequence could enhance assay performance. To test this, we introduced an additional guide DNA targeting the antisense strand of the mutant allele for selective nicking. Compared to the single-guide DNA setup, fluorescence signals increased; however, the assay failed to distinguish the mutant allele (Fig. 2, A to E). A likely explanation is that the guide DNA targeting the antisense strand formed a quaternary complex with the activator and Cas12a-crRNA, which disrupted specific recognition. Next, we compared and optimized the concentrations of both fluorescence ssDNA reporters and activators. We found that using a higher concentration of reporters and a lower concentration of activators produced the strongest fluorescence signal, characterized by an increase over time (figs. S2 and S3). We further evaluated the optimized assay by systematically controlling the reaction composition (fig. S4). We observed the highest analytical signal only when all components (nicked target DNA, Cas12a, crRNA, and activator) were present, whereas omission of any single component abolished the signal, confirming assay specificity.

After validating the assay design, we proceeded to optimize the one-pot RPA-*TtAgo* reaction (Fig. 2F), in which RPA amplification and *TtAgo* cleavage occur in the same tube but are spatially separated through density regulation by glycerol. First, we evaluated the fidelity of RPA amplification to ensure that no amplification errors were introduced. Sanger sequencing confirmed the high fidelity of RPA in preserving the target mutation sequence (fig. S5). We then

Downloaded from https://www.science.org on May 23, 2026

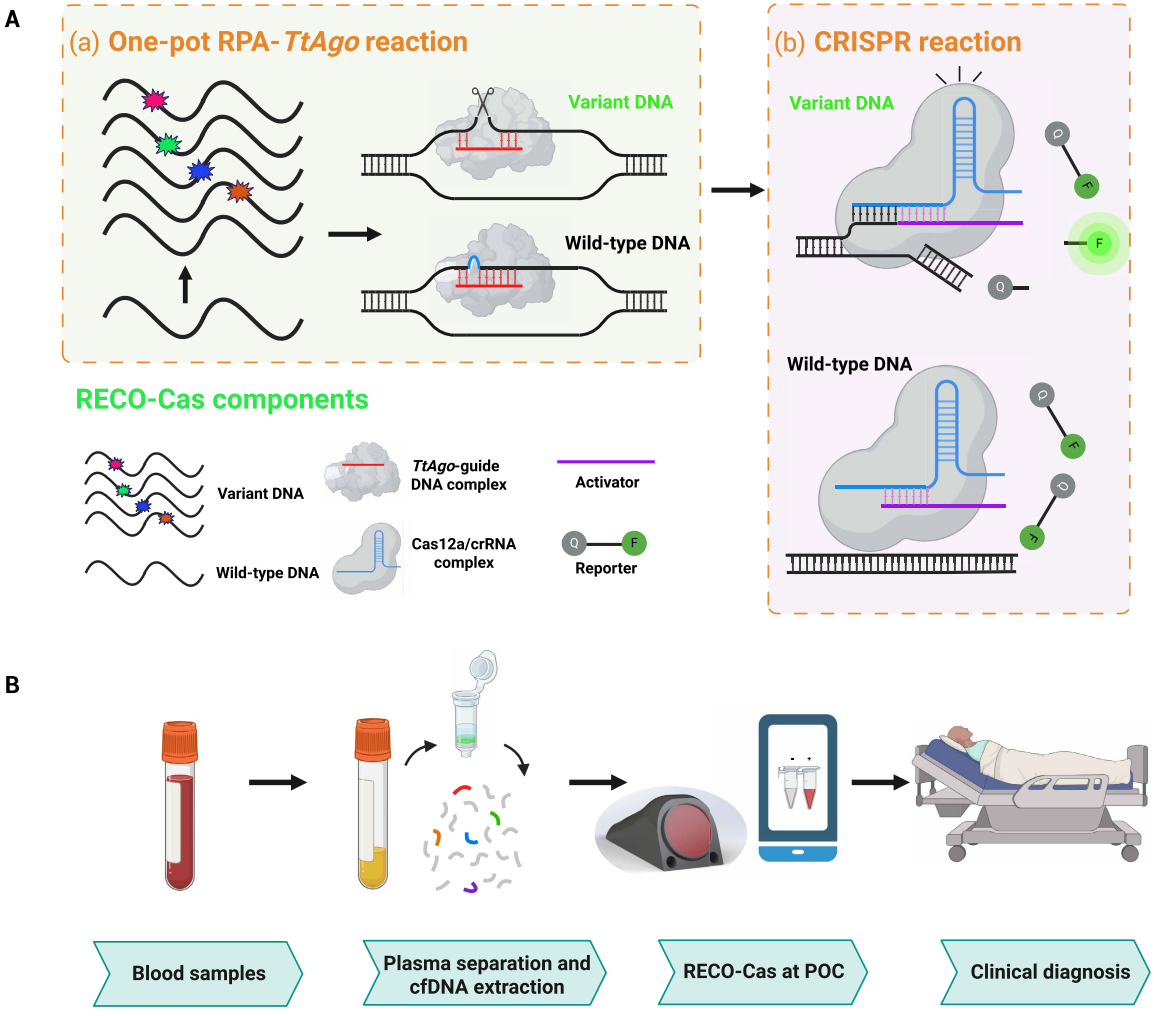


Fig. 1. RECO-Cas. (**A**) RECO-Cas mechanism. The assay combines a one-pot RPA-*TtAgo* reaction with mutation-specific Cas12a trans-cleavage detection: (a) cfDNA is first amplified by RPA, after which the *TtAgo*-guide DNA complex selectively recognizes and cleaves the mutant amplicons, introducing a nick into mutant DNA while leaving wild-type DNA intact. (b) The resulting nicked product is introduced into the Cas12a reaction, containing the ssDNA activator and Cas12a-crRNA. Cas12a-crRNA specifically recognizes the recombined construct of the ssDNA activator and nicked mutant DNA, forming a quaternary complex that activates Cas12a trans-cleavage of a fluorophore-quencher reporter, thereby generating a fluorescence signal. (**B**) RECO-Cas workflow for POC diagnostics using a compact, wirelessly powered diagnostic platform and an AI-powered smartphone. The assay produces molecular information within ~60 min, enabling same-day clinical diagnosis. Created in BioRender. C. Guo (2026), https://biorender.com/e5zim2v.

optimized the concentration of *TtAgo* to maximize signal intensity (Fig. 2, G and H). In Fig. 2G, we monitored real-time fluorescence from the one-pot RPA-*TtAgo* reaction using a single guide DNA while varying *TtAgo* concentrations. Higher concentrations of *TtAgo* consistently produced stronger fluorescence signals ($P < 0.001$). In Fig. 2H, to generate an analyzable DNA sequence for Sanger sequencing, we used dual guide DNAs targeting both strands of the mutant allele, with the amount of *TtAgo* enzyme doubled accordingly. The results were consistent with the fluorescence data, showing that nearly all mutant alleles were cleaved. In addition, discriminatory cleavage of the mutant sequence was not affected in the one-pot reaction system (Fig. 2I). Because high-viscosity glycerol can potentially affect RPA amplification (*32*), we next determined the effect of glycerol concentration on the one-pot RPA-*TtAgo* reaction. As shown in Fig. 2J, fluorescence readouts differed significantly among conditions ($P < 0.001$). A 10% glycerol layer produced the strongest signal, whereas 5% glycerol did not improve fluorescence, and 20% glycerol substantially inhibited the RPA reaction. The likely explanation is that lower-viscosity solutions permit RPA components to diffuse rapidly into the *TtAgo* layer, partially inhibiting cleavage. Consistent with this hypothesis, Sanger sequencing in Fig. 2K confirmed reduced *TtAgo* activity in reactions containing 5% glycerol. Overall, these optimizations established the optimal conditions for RECO-Cas, ensuring robust performance in cfDNA mutation detection.

RECO-Cas assay characterization

RECO-Cas achieved high selectivity through the specific recognition of crRNA, activator, and nicked mutant alleles, enabling reliable analysis of cfDNA samples with low VAFs. Using the optimized protocol, we assessed the assay's analytical performance across a range of VAFs. We detected the $KRAS^{G12D}$ mutant allele in both synthetic oligonucleotides and diluted cfDNA reference standards at a VAF as

Downloaded from https://www.science.org on May 23, 2026

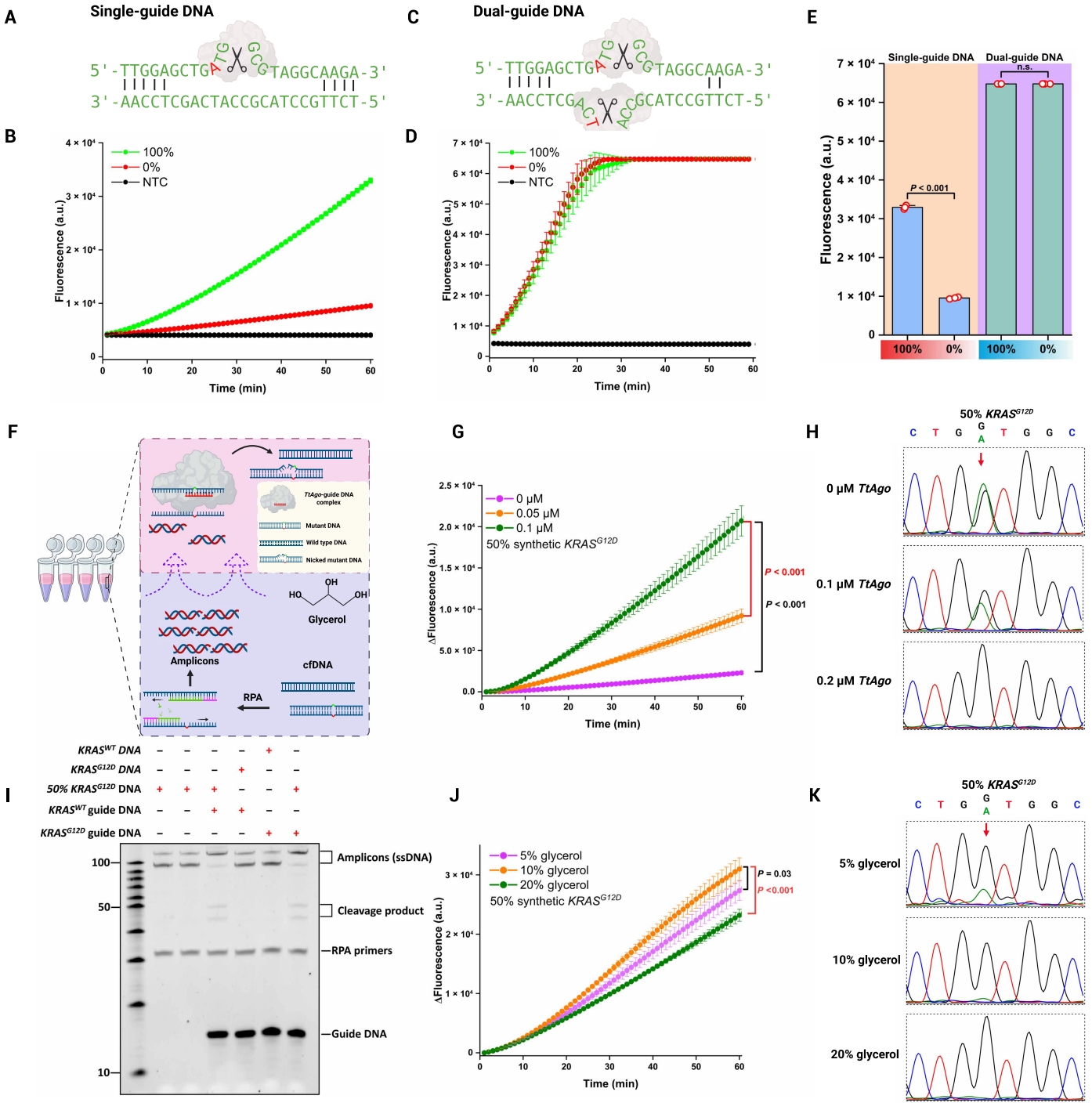


Fig. 2. Optimization of the one-pot RPA-*TtAgo* reaction. (**A**) Schematic of the single-guide DNA bound to the *KRAS*^{G12D} target sequence, highlighting the single mismatch at the mutation site (T/G). The cleavage site is indicated by scissors. (**B**) Real-time fluorescence signals over time for samples containing 100% mutant (green), 0% mutant (wild type; red), and no-template control (NTC; black). a.u., arbitrary units. (**C**) Schematic of dual-guide DNA complexes targeting both flanks of the *KRAS*^{G12D} sequence, increasing detection sensitivity. (**D**) Real-time fluorescence signals showing weak discrimination between 100% mutant and 0% mutant samples. The reaction exhibited a steep increase in fluorescence for both the mutant and wild type but no end point distinction. (**E**) End point fluorescence signal after 60 min for the 100 and 0% *KRAS*^{G12D} fractions. (**F**) Schematic illustration of the one-pot RPA-*TtAgo* reaction. The inset shows an image of the reaction components and final product within the one-pot setup. (**G**) Real-time fluorescence signals of 50% synthetic *KRAS*^{G12D} samples treated with varying concentrations of *TtAgo*. (**H**) Comparison of Sanger sequencing chromatograms of synthetic 50% *KRAS*^{G12D} samples after treatment with different concentrations of *TtAgo* in the one-pot RPA-*TtAgo* reaction. (**I**) Denaturing polyacrylamide gel electrophoresis of degradation products from synthetic *KRAS*^{G12D} and *KRAS*^{WT} targets in the one-pot RPA-*TtAgo* reaction. (**J**) Effect of glycerol concentration on the RPA-*TtAgo* reaction. (**K**) Comparison of Sanger sequencing chromatograms of one-pot reaction products with varying glycerol concentrations. Created in BioRender. C. Guo (2026), https://biorender.com/e5zim2v.

Downloaded from https://www.science.org on May 23, 2026

low as 0.01% (Fig. 3A and figs. S6 and S7), demonstrating performance comparable to digital PCR and sequencing (*17*, *33*). RECO-Cas achieved attomole-level sensitivity for synthetic $KRAS^{G12D}$ with performance comparable to TaqMan PCR (Fig. 3B). Because the two assays use different fluorescent reporters and thus have distinct background levels, we quantified Δfluorescence (end point minus baseline) as a normalized readout to enable a fair comparison. This high analytical sensitivity enables the reliable detection of rare mutations in low-input samples such as plasma-derived cfDNA.

Notably, RECO-Cas also demonstrated excellent sequence specificity, enabling precise classification of single-nucleotide missense mutations. Given that *KRAS* is one of the most frequently studied oncogenic drivers in cancer, we selected it as a model target to evaluate the detection specificity of RECO-Cas. To assess its ability to discriminate between sequences differing by a single nucleotide, we specifically designed guide DNAs and crRNAs for $KRAS^{WT}$ and three clinically relevant mutant subtypes, including $KRAS^{G12D}$, $KRASG^{12V}$, and $KRAS^{G12A}$ (figs. S8 to S10). RECO-Cas consistently produced high signal-to-background ratios, effectively distinguishing on-target from off-target samples even at VAFs as low as 1% with target concentrations of 50 nM (Fig. 3C). To demonstrate its versatility, we also designed and validated guide DNAs targeting $EGFR^{L858R}$ and $PIK3CA^{E545K}$, demonstrating excellent nicking specificity (figs. S11 and 12). Leveraging Cas12a's tolerance for short ssDNA activators and the exceptional specificity of crRNA, we developed a multiplexed RECO-Cas platform that enables simultaneous identification of diverse mutant alleles. To create a multiplexed RECO-Cas assay, we performed *TtAgo* cleavage on all three target mutant alleles in a single tube and then distributed the reaction into three separate tubes for the subsequent CRISPR detection. Each mutant allele was present at a concentration of 50 nM (Fig. 3D and fig. S13). Collectively, these results highlight the potential of RECO-Cas for accurate SNV mutation detection and classification with high sensitivity and specificity.

Multicancer early detection

Circulating cfDNA liquid biopsy has emerged as a promising noninvasive approach for early cancer detection across multiple tumor types; however, its clinical utility is limited by low ctDNA levels in early-stage disease, reduced sensitivity in low-shedding tumors, and challenges in distinguishing malignant from benign signals (*6*, *34*–*36*). We therefore hypothesized that the high sensitivity of RECO-Cas could enable early cancer detection through cfDNA liquid biopsy. To

Downloaded from https://www.science.org on May 23, 2026

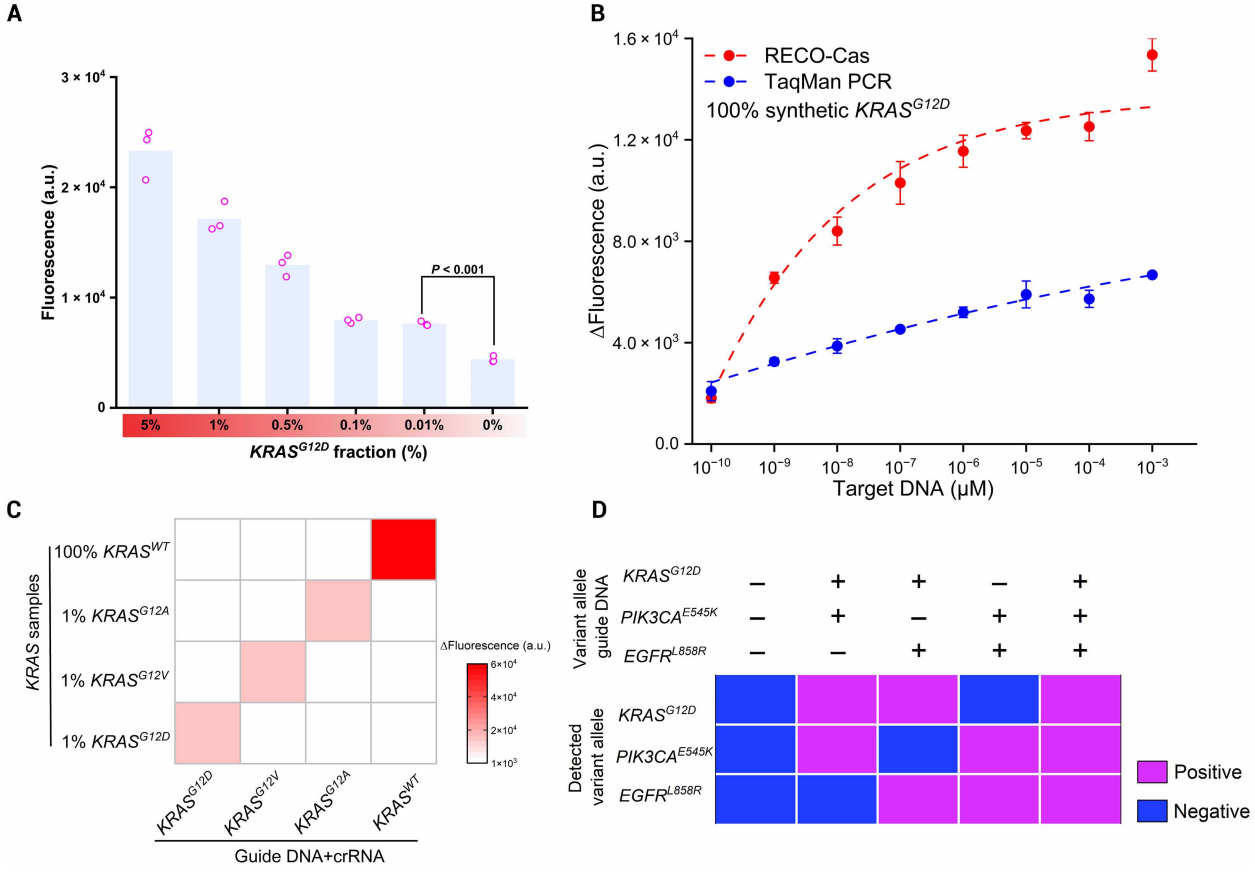


Fig. 3. RECO-Cas assay characterization. (**A**) A mixture of $KRAS^{WT}$ and $KRAS^{G12D}$ synthetic DNA was prepared at varying VAFs. RECO-Cas detected $KRAS^{G12D}$ down to 0.01% VAF, yielding a signal significantly above the background ($P < 0.001$). (**B**) RECO-Cas (70 min) and TaqMan PCR (45 cycles) detected synthetic $KRAS^{G12D}$ at varying concentrations. Bars represent mean values from technical triplicates. ΔFluorescence: end point fluorescence minus baseline. (**C**) The specificity of guide DNA and crRNA targeting $KRAS^{WT}$ and $KRAS^{G12D}$, $KRAS^{G12A}$, or $KRAS^{G12V}$ was assessed. At a target concentration of 50 nM, RECO-Cas produced high signal contrast between matched and mismatched targets. The heatmap displays mean values from technical triplicates. (**D**) Multiplex mutation detection of $KRAS^{G12D}$, $PIK3CA^{E545K}$, and $EGFR^{L858R}$ by RECO-Cas. Blue rectangles indicate a negative signal, and pink rectangles indicate a positive signal.

test this, we applied RECO-Cas to detect cfDNA samples from patients who have cancer with confirmed *KRAS/PIK3CA/EGFR* missense mutations ($KRAS^{G12D}$, $KRAS^{G12V}$ $KRAS^{G12A}$, $PIK3CA^{E545K}$, and $EGFR^{L858R}$; table S1) and from healthy donors.

We first validated the detection performance of RECO-Cas using a commercial non–small cell lung cancer ctDNA reference standard and a wild-type negative control. We evaluated three primer sets that generated amplicons of different lengths and found that the 94–base pair amplicons produced stronger fluorescence signals in the RECO-Cas assay (fig. S14), consistent with the ~167–base pair mononucleosomal size distribution of plasma cfDNA, which favors shorter targets (*37*–*40*). We monitored time-resolved fluorescence signals (Δfluorescence) for both $KRAS^{G12D}$ and $KRAS^{WT}$ fragments (fig. S15). RECO-Cas produced consistently higher fluorescence for the $KRAS^{G12D}$ fragment, with a variant/wild-type ratio of 0.14, compared to 0.05 in the negative control. These data show that cfDNA from the reference standard produced a robust RECO-Cas signal for $KRAS^{G12D}$ detection, confirming reliable detection of this missense mutation.

We then applied RECO-Cas to analyze cfDNA extracted from plasma samples of patients with cancer. We collected and tested samples with confirmed *KRAS* missense mutations ($KRAS^{G12D}$, $KRAS^{G12V}$, and $KRAS^{G12A}$; $n = 18$). As a control, we assessed cfDNA samples extracted from healthy donors ($n = 10$). To establish the negativity threshold of the ratio for determining whether the assay identified a sample as positive for a *KRAS* mutation, we calculated the variant/wild-type ratio in patients who have cancer with $KRAS^{WT}$ ($n = 10$). We pooled the data from cfDNA samples without *KRAS* mutations and from healthy donors in a bar chart (fig. S16). We next set the threshold for *KRAS* mutation negativity as mean + 3 × standard deviation (SD) (threshold, 0.098). Applying this threshold, we effectively classified samples by *KRAS* mutation status, identifying 16 of 18 samples as *KRAS* mutation positive (Fig. 4A) and further resolving the specific *KRAS* mutation types present in each sample (Fig. 4B). In addition, we validated RECO-Cas in patients with cancer harboring $EGFR^{L858R}$ and $PIK3CA^{E545K}$ (Fig. 4A). Thus, the RECO-Cas assay demonstrated a sensitivity of 90.48% [95% confidence interval (CI): 69.62%, 98.83%] and a specificity of 100% (95% CI: 69.15%, 100%) in clinical samples. Receiver operating characteristic analysis showed high diagnostic performance, with an area under the curve of 0.972 (Fig. 4C). Overall, these findings highlight the potential of RECO-Cas for detecting early-stage tumors, minimal residual disease, and recurrence, particularly in cases with known mutations.

SNV detection of cfDNA

KRAS mutations are among the most common oncogenic alterations found in various cancers, including colorectal (*41*), lung (*42*), and pancreatic cancer (*43*). *KRAS* mutations promote tumor growth by activating key signaling pathways such as mitogen-activated protein kinase (*44*) and phosphatidylinositol 3-kinase (*45*). Identifying *KRAS* mutations is essential for guiding treatment, as *KRAS*-mutant cancers often resist *EGFR*-targeted therapies (*46*). With the rise of targeted therapies and clinical trials, identifying *KRAS* mutations through genotyping is essential for personalized cancer care. RECO-Cas offers a minimally invasive, accessible, and accurate approach for streamlined *KRAS* profiling. To determine the feasibility of SNV detection, we applied RECO-Cas to analyze *KRAS* mutations, focusing on nucleotide substitutions at position c.35 that give rise to different missense variants ($KRAS^{G12D}$, $KRAS^{G12V}$, and $KRAS^{G12A}$) through distinct base changes.

We first validated the guide DNA and crRNA for *KRAS* RECO-Cas with synthetic nucleotides (Fig. 3C and fig. S17). We then applied RECO-Cas to a clinical study as outlined in Fig. 4D. We collected plasma samples from patients with cancer and extracted cfDNA using a spin column method. The extracted cfDNA was then subjected to the RECO-Cas assay using four pairs of guide DNAs and crRNAs targeting $KRAS^{WT}$, $KRAS^{G12D}$, $KRAS^{G12V}$, and $KRAS^{G12A}$. Figure 4 (E and F) shows the identification of *KRAS* missense variants in the ctDNA reference standard using the RECO-Cas assay. The variant/wild-type ratios for $KRAS^{G12D}$ and $KRAS^{G12V}$ were 0.264 and 0.124, respectively, both exceeding the detection threshold. These results confirmed successful detection of $KRAS^{G12D}$ and $KRAS^{G12V}$ mutations, consistent with the mutation types documented in the reference standard manual. In contrast, assays using guide DNA + crRNA targeting $KRAS^{G12A}$ or nonguide DNA + $KRAS^{WT}$ crRNA yielded variant/wild-type ratios below the threshold, consistent with the $KRAS^{G12A}$-negative status of the reference material. These observations support the rationale for assessing tumor *KRAS* missense variants using RECO-Cas profiling.

We further validated the classification of tumor missense variants in 18 patients who have cancer with *KRAS* mutations ($KRAS^{G12D}$, $n = 9$; $KRAS^{G12V}$, $n = 5$; $KRAS^{G12A}$, $n = 4$) using RECO-Cas. cfDNA samples were subjected to RECO-Cas analysis with four pairs of guide DNAs and crRNAs, each targeting a specific *KRAS* missense variant as well as the wild-type sequence. Figure 4G shows the performance of RECO-Cas in classifying *KRAS* missense variants. In the $KRAS^{G12D}$ guide DNA and crRNA treatment group, eight of nine confirmed patients with $KRAS^{G12D}$ were correctly diagnosed, with one being false negative but no misclassifications from other mutation groups. For the $KRAS^{G12V}$ guide DNA and crRNA treatment, four of five patients with $KRAS^{G12V}$ were correctly identified, while one was misdiagnosed; additionally, one patient showed a variant/wild-type ratio above the threshold for both $KRAS^{G12D}$ and $KRAS^{G12V}$, resulting in dual positive signals. All patients with $KRAS^{G12A}$ mutations were accurately classified, and no patients with $KRAS^{G12D}$ or $KRAS^{G12V}$ were misclassified as $KRAS^{G12A}$. Results from several cases highlight the value of cfDNA mutation profiling for cancer diagnosis and guiding clinical therapy decisions. For example, a 65-year-old female diagnosed with colorectal cancer showed dual-positive signals of $KRAS^{G12D}$ and $KRAS^{G12V}$ by RECO-Cas (fig. S18), consistent with a case report describing the coexistence of $KRAS^{G12D}$- and $KRAS^{G12V}$-bearing subclones within the same tumor (*47*), indicative of intratumoral heterogeneity. Missense variant classification using RECO-Cas in patients with cancer could guide targeted therapy, for example, by identifying candidates for $KRAS^{G12D}$ inhibitors such as MRTX113 (*48*, *49*), currently in phase 1/2 clinical trials (NCT05737706) (*50*), thereby sparing patients from ineffective treatments like cetuximab or panitumumab (*51*) and supporting the selection of alternative or combination regimens following surgery. Furthermore, these SNV detection results highlight the potential of the RECO-Cas assay to develop a cfDNA-based prognostic metric to guide treatment selection, clinical trial enrollment, drug matching, and the duration of adjuvant therapy.

Integration of the RECO-Cas assay into a wirelessly powered POC diagnostic platform

Because of its simplicity, rapidity, and low cost (table S2), RECO-Cas is highly suitable for minimally instrumented, POC applications in resource-limited settings by integrating with a simple, compact

Downloaded from https://www.science.org on May 23, 2026

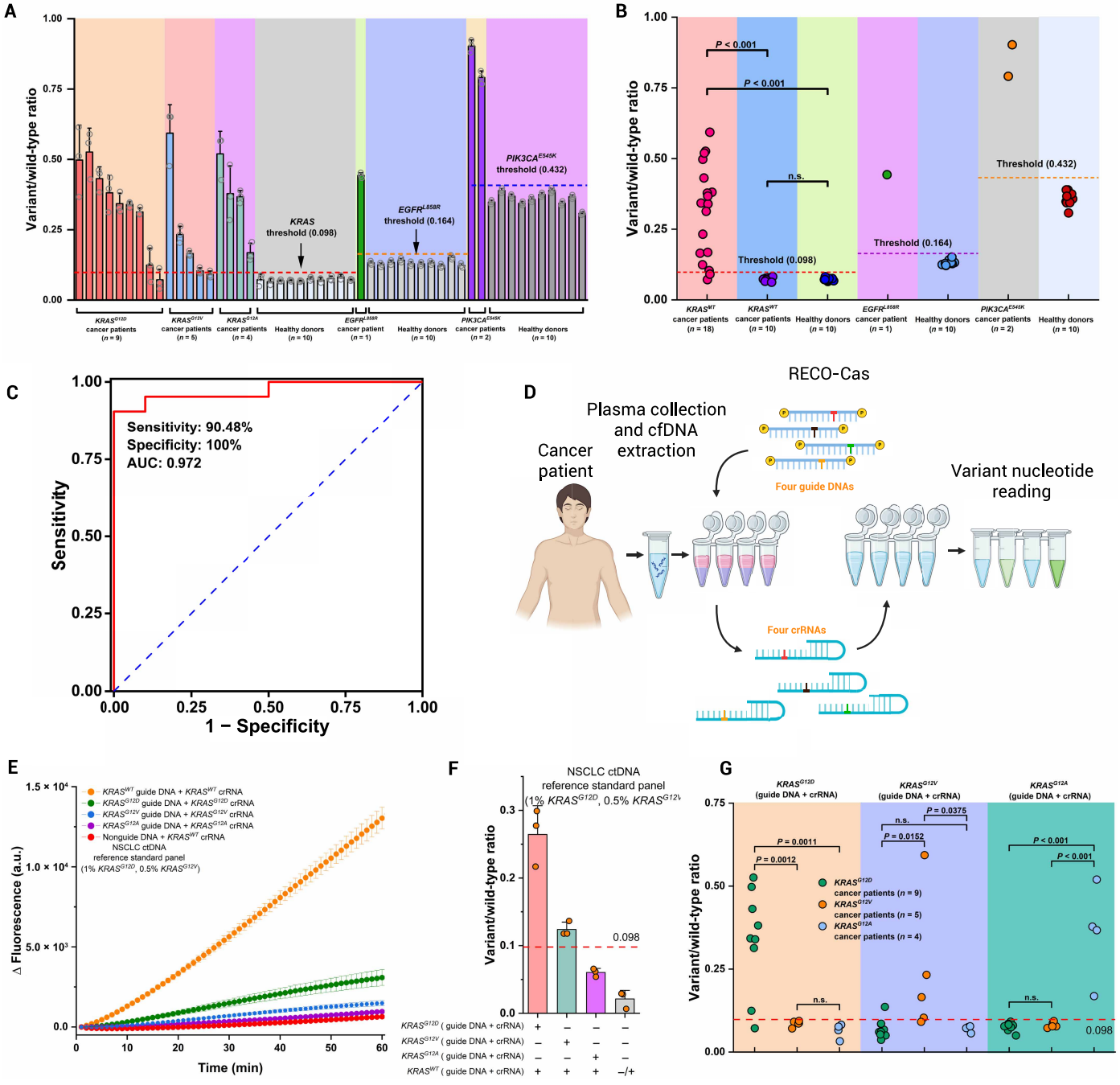


Fig. 4. Clinical validation of RECO-Cas. (**A**) Waterfall plot showing clinical assay of plasma collected from healthy donors ($n = 10$) and patients diagnosed with mutations: $KRAS^{G12D}$ ($n = 9$), $KRAS^{G12V}$ ($n = 5$), $KRAS^{G12A}$ ($n = 4$), $EGFR^{L858R}$ ($n = 1$), and $PIK3CA^{E545K}$ ($n = 2$). Data are displayed as the means ± SD from triplicate measurements. (**B**) The variant/wild-type ratio (= $KRAS^{MT}/KRAS^{WT}$) in patients with $KRAS^{MT}$ was substantially higher than in patients with $KRAS^{WT}$ (*wild-type KRAS*) and healthy donors ($P < 0.001$). Data are displayed as the means from triplicate measurements. (**C**) Receiver operating characteristic curve generated from the diagnosis results of 21 clinical samples and 10 healthy donors. AUC, area under the curve. (**D**) Workflow of RECO-Cas in mutant nucleotide sequencing. cfDNA was extracted from the plasma samples and amplificated by RPA, and amplicons were selectively cleaved by *TtAgo* in the presence of four pairs of guide DNAs. The cleavage product was then quantified by the Cas12a reaction. Real-time fluorescence analysis (**E**) and bar graph (**F**) demonstrating RECO-Cas detection of *KRAS* single-nucleotide missense mutations in ctDNA reference standards containing 1% $KRAS^{G12D}$ and 0.5% $KRAS^{G12V}$. With $KRAS^{G12D}$ and $KRAS^{G12V}$ guide DNAs, the variant/wild-type ratio exceeded both $KRAS^{G12A}$ guide DNA and nonguide DNA treatments, surpassing the predetermined positivity threshold, confirming that $KRAS^{G12D}$ and $KRAS^{G12V}$ are detectable in the ctDNA reference standard. (**G**) *KRAS* nucleotide sequencing results in patients with cancer. Amplicons from each patient were analyzed with four pairs of guide DNAs targeting $KRAS^{G12D}$, $KRAS^{G12V}$, $KRAS^{G12A}$, and $KRAS^{WT}$. Variant/wild-type ratios were collected. Two of 18 patients were misclassified as negative (false negatives), resulting in missed diagnoses; none of the patients were misclassified as carrying other synonymous substitutions. Data are the means from triplicate measurements. Created in BioRender. C. Guo (2026), https://biorender.com/e5zim2v.

Downloaded from https://www.science.org on May 23, 2026

diagnostic platform. To demonstrate its feasibility in such settings, we designed and developed a compact, 3D-printed diagnostic platform integrated with an AI-powered smartphone (Fig. 5A). The platform integrates a miniature heater for incubation and a light-emitting diode (LED) with fluorescence filters for signal detection. To enable convenient and continuous operation, the POC diagnostic platform can be wirelessly charged. To eliminate the need for expensive optical detection equipment, we programmed a smartphone with an AI-powered application for fluorescence recording, image processing, and quantitative fluorescence detection (Fig. 5A). To enhance the fluorescence signal and minimize background noise while maintaining a compact platform design, we placed the excitation filter beneath the reaction tubes and captured fluorescence images from the side through an emission filter (Fig. 5B). The AI-powered smartphone app uses an algorithm that identifies the region of interest (ROI) by tracing the contour of each PCR strip tube, thereby minimizing background interference. To further improve signal specificity, the app refines the ROI to exclude peripheral regions with mean pixel intensities indistinguishable from background noise. The finalized ROIs are then digitized for quantitative fluorescence analysis (Fig. 5C). We then evaluated the smartphone-based POC platform for its LoD using RECO-Cas reactions. We recorded fluorescence signals across serial dilutions of synthetic $KRAS^{G12D}$ sequences, with corresponding signal quantification shown in Fig. 5D. For each clinical sample, we measured two fluorescence signals using the platform: one corresponding to the wild-type allele and the other to the variant sequence. We applied the ratio of variant to wild-type fluorescence intensity to determine the patient's status as either healthy or cancer-diagnosed. Using this protocol, we analyzed a dilution series of $KRAS^{G12D}$ in a $KRAS^{WT}$ background and observed a broad, nonlinear detection range from 0.01 to 100% $KRAS^{G12D}$, showing good performance of the prototype platform for mutant nucleotide detection. Notably, we detected significant differences between the 0.01 and 0% groups, even when fluorescence signals were not visually discernible in the captured images (Fig. 5E).

As a proof of concept for clinical applications, we first evaluated the POC platform to detect *KRAS* mutations in cfDNA extracted from plasma samples of three healthy donors and nine patients who have cancer with *KRAS* single-nucleotide missense mutations ($KRAS^{G12D}$, $n = 3$; $KRAS^{G12V}$, $n = 3$; $KRAS^{G12A}$, $n = 3$). We tested cfDNA samples from healthy donors using $KRAS^{WT}$ and $KRAS^{G12D}$ guide DNA and crRNA, and we treated the cfDNA from patients who have cancer with mutation-matched guide DNA and crRNA targeting their respective *KRAS* variants. As shown in Fig. 5 (F and G), the platform successfully detected mutations in the captured images and distinguished patients with cancer from healthy donors, consistent with the diagnostic results obtained from RECO-Cas assays performed on a quantitative PCR (qPCR) machine. In addition to detecting known mutations, we further validated the platform's ability to classify single-nucleotide missense mutations. We treated a ctDNA reference standard with four pairs of guide DNA and crRNA, and the resulting fluorescence images (fig. S19) confirmed accurate classification of the mutant nucleotides by the diagnostic platform, consistent with the results obtained from qPCR machine analysis. To assess clinical applicability, we applied the platform to detect cfDNA samples extracted from healthy donors and patients who have cancer with known *KRAS* mutations. The compact diagnostic platform successfully classified all patients with cancer (Fig. 5, H and I, and fig. S20), demonstrating reliable mutation discrimination in a clinical context. In summary, this proof-of-concept study demonstrates the potential of the compact POC diagnostic platform as a simple, low-cost, and scalable solution for developing next-generation molecular diagnostic tools for cancers, particularly in resource-limited or decentralized health care settings.

DISCUSSION

Our results indicate the potential of the RECO-Cas diagnostic platform as a user-friendly and highly specific platform for detecting cancer-associated SNVs of cfDNA in liquid biopsy, overcoming limitations of mismatch tolerance in Cas12a and lack of signal amplification in *TtAgo*-based systems. We evaluated the clinical performance of RECO-Cas using plasma samples from patients with cancer and healthy donors. The platform successfully detected mutant alleles at 0.01% VAF, demonstrating ultrasensitive detection capabilities. In a proof-of-concept study involving 21 samples from patients with cancer and 10 healthy donors, RECO-Cas detected mutant cfDNA in 19 samples and achieved a clinical sensitivity of 90.48% (95% CI: 69.62 to 98.83%) and a specificity of 100% (95% CI: 69.15 to 100%). Notably, we validated the performance of RECO-Cas in discriminating single-nucleotide missense mutations at the *KRAS* locus using 18 clinical plasma samples. Among these, 16 samples were accurately classified according to their known mutation status. One sample was identified as dual-positive for both $KRAS^{G12D}$ and $KRAS^{G12V}$.

Previous approaches have applied either Cas12a-based signal amplification or Argonaute-mediated mutation discrimination, yet each alone suffers from key limitations—mismatch tolerance and lack of signal amplification (*26*, *27*, *29*, *30*, *52*). Most of these methods require a separate DNA degradation step or involve additional procedures to identify the mutant sequence, which limits their applicability in resource-limited settings. For example, the NAVIGATER assay achieves ultrasensitive detection of mutant alleles (~1 copy) for cancer diagnosis but relies on two distinct steps, cfDNA amplification and wild-type sequence degradation, and requires xeno nucleic acid PCR for mutation identification, which constrains its practicality for clinical settings (*30*). An Argonaute-integrated single-tube PCR system enables ultrasensitive detection of rare mutations by combining preamplification and wild-type sequence degradation in a single reaction. However, the reliance on thermal cycling and complex instrumentation for mutation identification limits its applicability in POC settings (*29*). Last, an RPA-based ID-CRISPR assay detected the $EGFR^{L858R}$ mutation with a 0.1% VAF LoD, which remains less sensitive than established methods. The reduced specificity stems from Cas12a's high mismatch tolerance, allowing cleavage of near-target sequences and effectively limiting the LoD for SNV detection (*53*, *54*). Compared with the widely used ddPCR platform, RECO-Cas differs across multiple critical resource dimensions—including overall workflow complexity, labor requirements, key reagents, per-sample reagent cost, required equipment, sample throughput, runtime, sensitivity, and quantification capability (table S3). In contrast, in the RECO-Cas assay described here, we integrated the one-pot RPA-*TtAgo* cleavage reaction with trans-cleavage signal amplification by CRISPR-Cas12a, allowing this platform to provide a simple, highly sensitive, and specific approach for mutation profiling directly from cfDNA, advancing its utility in precision oncology and liquid biopsy.

cfDNA is a rich source of tumor-derived molecular information and enables accurate cancer diagnosis across various stages (*55*). Mutant cfDNA levels typically decrease after treatment initiation and remain stable or rise during resistance or disease progression,

Downloaded from https://www.science.org on May 23, 2026

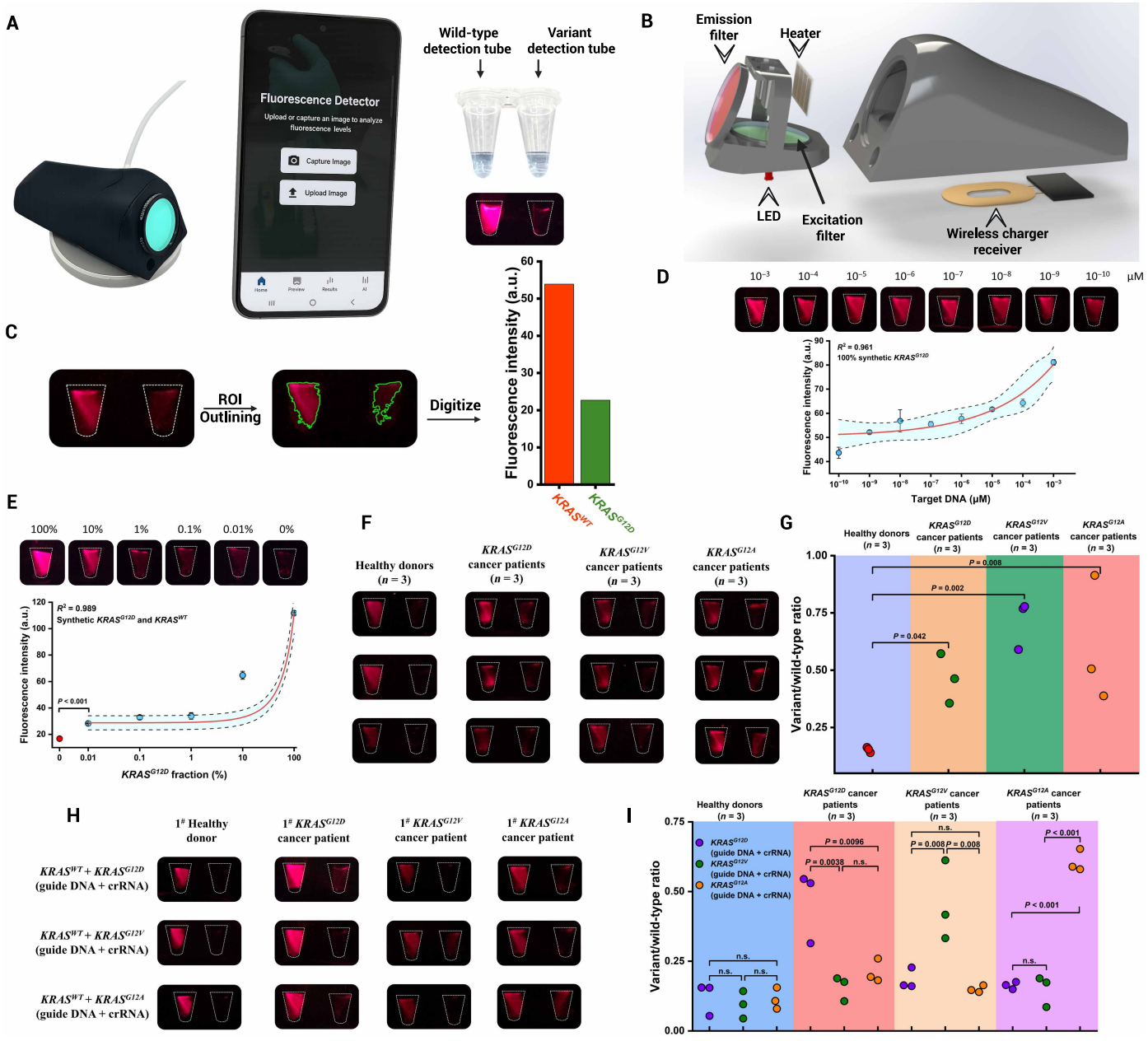


Fig. 5. Assessment of the RECO-Cas assay for POC testing by a compact wirelessly powered diagnostic platform integrated with an AI-enabled smartphone. (**A**) Photograph of a compact, wirelessly powered prototype platform for CRISPR-based fluorescence detection using an AI-powered smartphone app. End point fluorescence image of a *KRAS*^{WT} sample treated with either *KRAS*^{WT} guide DNA (right) or *KRAS*^{G12D} guide DNA (left). The white dotted line represents the fixed position of the RECO-Cas reagents. (**B**) 3D schematic rendering of the POC diagnostic platform, illustrating its key components. (**C**) Workflow for optimizing ROI detection. (**D**) Representative end point fluorescence images (top) and corresponding standard curve (bottom) for detection of synthetic *KRAS*^{G12D} at varying concentrations. Data are shown as the means ± SD ($n = 3$). (**E**) Representative end point fluorescence images (top) and corresponding standard curve (bottom) for detection of synthetic *KRAS*^{G12D} in a background of *KRAS*^{WT} across a dilution series (0.01 to 100%). Data are shown as the means ± SD ($n = 3$). (**F** and **G**) Representative end point fluorescence images (F) and scatter dot plots (G) for detecting three *KRAS* mutations in cfDNA extracted from plasma samples of healthy donors ($n = 3$) and patients who have cancer with *KRAS*^{G12D}, *KRAS*^{G12V}, or *KRAS*^{G12A} ($n = 3$ each) using the RECO-Cas platform. Scatterplots were generated from background-corrected mean fluorescence intensities normalized to the *KRAS*^{WT} guide DNA signal: variant/wild-type = fluorescence (variant guide DNA)/fluorescence (wild-type guide DNA). (**H**) Representative end point fluorescence images for classifying three *KRAS* SNVs in cfDNA extracted from plasma samples of healthy donors and patients who have cancer with *KRAS*^{G12D}, *KRAS*^{G12V}, or *KRAS*^{G12A} using the RECO-Cas platform. (**I**) Scatterplots presenting sequencing of *KRAS* SNVs in cfDNA extracted from plasma samples of healthy donors ($n = 3$) and patients who have cancer with *KRAS*^{G12D}, *KRAS*^{G12V}, or *KRAS*^{G12A} ($n = 3$ each) using the RECO-Cas platform. Data are the means from triplicate measurements.

Downloaded from https://www.science.org on May 23, 2026

supporting its utility for monitoring therapeutic response and disease dynamics (*56*, *57*). Despite its value, plasma cfDNA is often present at very low concentrations and is diluted by abundant wild-type cfDNA, posing challenges for sensitive detection (*58*). Given these attributes, cfDNA-based assays are considered highly promising for noninvasive cancer diagnostics despite their reliance on complex sample processing steps such as mutation enrichment and high-throughput sequencing (*18*, *23*, *59*). The RECO-Cas technology can overcome these limitations by coupling one-pot RPA-*TtAgo* reaction with CRISPR detection. (i) RECO-Cas achieves single-nucleotide specificity through mismatch-intolerant enzymatic cleavage by *TtAgo*. (ii) RECO-Cas integrates RPA amplification with *TtAgo* cleavage in a one-pot format to streamline the workflow. (iii) The isothermal reaction conditions and Cas12a-based fluorescence readout make the platform well suited for POC applications. These advantages support the integration of RECO-Cas into routine preclinical and clinical workflows.

The clinical validation results highlight the clinical potential of RECO-Cas as a precision diagnostic tool for guiding targeted cancer therapies through accurate cfDNA-based mutation profiling. RECO-Cas achieves single-nucleotide resolution at the *KRAS* locus and fulfills a critical need for selecting and monitoring patients eligible for mutation-specific treatments, such as MRTX1133 and QTX3034 for advanced solid tumors harboring $KRAS^{G12D}$ (*50*, *60*), or combination therapies like vebreltinib and osimertinib in patients with $EGFR^{L858R}$-mutated non–small cell lung cancer (*61*). RECO-Cas distinguishes closely related missense mutations directly from plasma cfDNA and enhances its utility in refining therapeutic decision-making, particularly in cancers where mutation subtype dictates drug sensitivity or resistance. In addition, the detection of dual-positive samples suggests that RECO-Cas may also capture intratumoral heterogeneity and subclonal variation, factors increasingly recognized as critical determinants of treatment response and disease progression (*62*). With its high sensitivity, single-nucleotide specificity, and operational simplicity, RECO-Cas offers a promising solution for routine clinical implementation in early diagnosis, therapy selection, and longitudinal monitoring of minimal residual disease.

The future of cancer diagnostics lies in systems that can resolve clinically actionable mutations from minute amounts of cfDNA with minimal instrumentation, enabling real-time decision-making across diverse health care settings. Therefore, we developed a compact, wirelessly powered, smartphone-based POC diagnostic platform to demonstrate a minimally instrumented RECO-Cas assay. The development of the POC platform demonstrates the engineering versatility and translational potential of the RECO-Cas assay. By integrating a wireless power receiver, a miniature incubator, LED-based fluorescence excitation, optical filtering, and a smartphone app for automated image analysis, the platform minimizes the need for instrumentation and enables user-friendly operation suitable for decentralized clinical environments. This platform successfully detected and classified *KRAS* SNVs across a wide dynamic range, from 0.01 to 100% VAF and at attomole input levels, illustrating both high analytical sensitivity and broad clinical applicability. The assay results obtained from the compact platform were consistent with those from a standard qPCR machine, validating its diagnostic accuracy. This integrated POC platform substantially lowers the barrier for implementing cfDNA mutation testing in low-resource settings, making it well suited for use in early cancer detection, treatment monitoring, and personalized oncology applications.

Previous studies analyzing mutant nucleic acids, including mRNA, suggest that mutation levels may correlate with posttherapy clinical outcomes (tumor-free status) (*63*). Because of the lack of posttreatment samples from patients with cancer, such as those collected following surgery or chemotherapy, we could not assess the utility of RECO-Cas for monitoring treatment response. Although RECO-Cas reliably identifies low-frequency mutant alleles, precise VAF quantification remains beyond the scope of this assay and should be determined using established quantitative methods (e.g., ddPCR or NGS) when clinically required. In addition, cfDNA is wrapped around histone proteins in the form of mono-, di-, or trinucleosomes, which introduces added complexity to the extraction process (*37*, *64*). Beyond this biochemical challenge, plasma separation itself requires careful handling, as whole blood must be processed promptly through sequential low- and high-speed centrifugation steps to prevent cellular lysis and contamination with genomic DNA. This presents a substantial challenge for integrating cfDNA extraction and detection into a unified, single system. Establishing clinical datasets that include posttreatment time points and streamlined methods to release and purify cfDNA from its nucleosome structure will further clarify how RECO-Cas can be applied across the continuum of cancer care, from diagnosis to longitudinal monitoring. Last, our approach has diagnostic implications, as it enables the detection and classification of single-nucleotide missense mutations through a streamlined workflow that is compatible with POC integration.

MATERIALS AND METHODS

Study design

The objective of this study is to develop and validate a rapid, sensitive diagnostic platform of RECO-Cas for SNV profiling of cfDNA from the plasma of patient with cancer, with the goal of enabling same-day results to support clinical decision-making. We hypothesize that a recombined DNA construct generated from Argonaute-nicked mutant DNA and ssDNA activator could selectively trigger CRISPR-Cas12a, thereby amplifying the fluorescence signals. This assay is expected to improve assay speed and reduce costs compared to conventional technologies such as ddPCR and NGS. A secondary objective of this study is to evaluate the performance of the RECO-Cas assay when integrated into a cost-effective POC diagnostic platform. The samples are from the group of patients with cancer (n = 21) and a control group. The control group consisted of healthy donors with no history of cancer. With the cohort in this study, the observed sensitivity and specificity were 90.48% (95% CI: 69.62%, 98.83%) and 100% (95% CI: 69.15%, 100%). All participants provided informed consent. All samples were measured at least three times (technical replicates), and the mean values were used for analyses. This study was approved by the Institutional Review Board of the University of Connecticut Health Center (IRB# 08-310-1), and the overall procedures followed institutional guidelines.

Reagents

Betaine, glycerol, Tween 20, and ACS reagent–grade urea were purchased from Sigma-Aldrich (St. Louis, MO). The TwistAmp Basic RPA kit was obtained from TwistDx (Maidenhead, UK). Tris-borate EDTA (TBE) buffer (10×), 40% acrylamide/bis-acrylamide solution (19:1), tetramethylethylenediamine, and ammonium persulfate were purchased from Bio-Rad Laboratories (Hercules, CA). EnGen Lba Cas12a (Cpf1) was purchased from New England Biolabs (Ipswich, MA).

Downloaded from https://www.science.org on May 23, 2026

VAF sample preparation

The 100-nucleotide target DNA sequences, guide DNA, and crRNA were purchased from Integrated DNA Technologies Inc. (Coralville, IA). Sense and antisense ssDNAs were incubated in hybridization buffer and gradually annealed by cooling from 95° to 37°C in 0.5°C increments every 2 min. Variant and wild-type DNA fragments were mixed to generate various VAFs for each allele to evaluate the detection performance of RECO-Cas.

TaqMan polymerase chain reaction

PCR primers and probe are listed in table S4. All PCR reactions were set up using Luna Universal Probe qPCR Master Mix (New England Biolabs, M3004X). Each reaction contained 5 μl of 2X Master Mix, 0.5 μl of forward primer, 0.5 μl of reverse primer, 0.5 μl of DNA probe (each at a 10 μM working concentration in nuclease-free water), 1 μl of template with confirmed concentration, and 2.5 μl of nuclease-free water. The thermocycling protocol included the following steps: 95°C for 2 min, 45 cycles of 95°C for 30 s, and 60°C for 30 s.

Standard RPA and one-pot RPA-*TtAgo* cleavage reaction

RPA reaction cocktails were generated by adding 10.5 μl of nuclease-free water, 2.5 μl of 10 μM forward primer, 2.5 μl of 10 μM reverse primer, and 29.5 μl of primer-free rehydration buffer to an RPA pellet and then adding 2.5 μl of 280 mM magnesium acetate to start DNA amplification. The one-pot system was prepared separately as components A and B. Component A contained 500 nM of each primer, 14 mM $MgSO_4$, 4 μl of 50% glycerol, and 2.5 μl of cfDNA in a total 20-μl reaction system. Component B contained 20 mM tris-HCl, 10 mM $(NH_4)_2SO_4$, 10 mM KCl, 8 mM $MgSO_4$, 0.1% Triton X-100, 0.1% Tween 20, 0.8 M betaine, 50 to 200 nM *TtAgo*, and 0.5 to 2 μM guide DNA in a total 20-μl reaction system. In the one-pot assay, 20 μl of component B was first added into the tube and briefly centrifuged, then 19 μl of component A was added to the bottom of the tube, and last, 1 μl of 280 mM magnesium acetate was added. The reaction was carried out at 39°C for 10 min and 83°C for 10 to 30 min, and the reaction mixture was cooled to 4°C. The upper phase of the reaction mixture was collected for the CRISPR-Cas12a assay.

Gel electrophoresis

Denaturing and native 12% polyacrylamide gel electrophoresis were performed to evaluate the discriminatory cleavage efficiency of *TtAgo* in recognizing mutant versus wild-type nucleotides. This included analysis of guide DNAs bearing single-nucleotide mismatches, mutant alleles targeted by guide DNAs, and RPA products. To prepare the denaturing gel, 12 g of urea was dissolved in a solution containing 7.5 ml of 40% acrylamide/bisacrylamide (19:1), 2.5 ml of 10× TBE buffer, and nuclease-free water was added to a final volume of 25 ml. Polymerization was initiated by adding 10 μl of tetramethylethylenediamine and 80 μl of 40% ammonium persulfate. The gel was stored at room temperature for at least 2 hours before use. Native gels were prepared using the same protocol, omitting urea. For cleavage product analysis, 5 μl of the reaction mixture was combined with 10 μl of 2× Gel Loading Buffer II (denaturing) and heated at 95°C for 10 min. A 10-μl aliquot of the mixture was then loaded onto the gel. As a size reference, 1 to 2 μl of ss10 DNA ladder mixed with 10 μl of 2× Gel Loading Buffer II was loaded into the first lane. Electrophoresis was conducted at a constant voltage of 300 V and an initial current of 25 mA for 1 hour. Gels were stained with SYBR Gold Nucleic Acid Gel Stain in 1× TBE buffer for 10 min, and nucleic acids were visualized using a Bio-Rad ChemiDoc MP imaging system.

Clinical sample collection, processing, and cfDNA extraction

Clinical samples from patients with lung, colon, and bladder cancers were collected at the University of Connecticut Health Center. Peripheral blood samples were collected from patients with cancer and healthy donors in accordance with published consensus guidelines for liquid biopsy preanalytical variables and reporting (*65*–*67*). Approximately 3 ml of whole blood was drawn into non–cell-stabilizing EDTA tubes. Blood samples were processed within a short time frame after collection to minimize leukocyte lysis. Plasma was isolated by an initial centrifugation step to separate cellular components, followed by a second high-speed centrifugation for 10 min to remove residual cellular debris. The clarified plasma was aliquoted and stored at −80°C until downstream analysis. Identical collection, processing, and storage procedures were applied to both patients with cancer and healthy donor controls, with no differences in tube type, blood volume, or centrifugation conditions. cfDNA was isolated with the QIAamp Circulating Nucleic Acid Kit (50-prep format; Qiagen, Hilden, Germany) according to the manufacturer's protocol. Briefly, 100 μl of plasma from each patient with cancer or healthy donor was diluted with 400 μl of phosphate-buffered saline and mixed with 50 μl of kit-supplied proteinase K and 400 μl of Buffer ACL, followed by incubation at 60°C for 30 min. The lysate was combined with 900 μl of Buffer ACB, loaded onto a QIAamp spin column, and centrifuged. Columns were washed sequentially with 600 μl of Buffer ACW1, 750 μl of Buffer ACW2, and 750 μl of 99% ethanol. cfDNA was eluted in 20 μl of Buffer AVE and quantified spectrophotometrically [A_{260} (absorbance at 260 nm)/A_{280}]. Eluates were stored at −80°C until analysis.

ddPCR

For each reaction, 1.5 μl of cfDNA was added to a 20 μl of ddPCR mixture containing 1× ddPCR Supermix for probes, 1.9 μM primers, and 250 nM of each of wild-type and mutant probes (table S4). Thermal cycling was conducted at 25°C for 3 min and 95°C for 10 min, followed by 40 cycles of 94°C for 30 s and 60°C for 1 min, with a final enzyme deactivation at 98°C for 10 min and a hold at 4°C for 3 min. After amplification, droplets were read on the QX200 system, and data were analyzed according to the manufacturer's instructions.

Sanger sequencing

Synthetic DNA was amplified using either standard RPA or a one-pot RPA-*TtAgo* cleavage reaction, as described above. A 1-μl aliquot of the 10^3-fold diluted amplified product was subsequently amplified using a hot-start PCR protocol. PCR products (10 μl) were purified and eluted in 30 μl using a DNA cleanup kit. Last, 10 μl of the purified PCR products was submitted for Sanger sequencing by Genewiz (US).

Wireless-powered POC diagnostic platform integrated with an AI-powered smartphone

The platform (32 mm by 35 mm by 70 mm) was designed using SolidWorks and fabricated by a Form 3 3D printer with black resin (RS-F2-GPBK-04, Formlabs, MA). The platform has two reaction tube wells in the miniature incubator for simultaneous detection of the variants and wild-type sequence. In the miniature incubator, a flexible thin-film heater (HK5572R26.5L23A, Minco, MN) and a thermocouple wire were fixed on its outer wall to heat the reaction

Downloaded from https://www.science.org on May 23, 2026

tubes and monitor the temperature, respectively (Fig. 5B). Power was supplied through a wireless charger receiver (MyMAX M1300, Amazon) attached to the bottom of the platform. For fluorescence imaging, the LED, excitation filter, and emission filter were selected to match the spectral properties of Cy5.

We also developed a smartphone app for image acquisition, image processing, and fluorescence quantification. For the fluorescence image analysis, the smartphone app automatically recognized and defined two ROIs in an RGB (red, green, and blue) image: one ROI for detection of the wild-type sequence and another ROI for detection of the variant. OpenCV detected the contour of each reaction tube and calculated mean pixel values inside the contour, excluding indistinguishable peripheral areas as background noise. For each test, the app presented raw images, ROI information, and quantitative fluorescence intensity data. The front end of the app was developed in JavaScript/TypeScript in React Native (via Expo), and the back end of the app was written in Python with a Django REST API.

Statistics

Statistical analysis was performed using OriginLab 2024 and MedCalc (https://www.medcalc.org/en/calc/diagnostic_test.php). Data are presented as the means ± SD, unless otherwise stated. Background-subtracted fluorescence values (fluorescence minus the value at time zero) are reported for all experiments, except for the assay optimization data, which are presented as total fluorescence values. Image-based fluorescence was quantified from end point fluorescence images. For comparisons among multiple groups, an analysis of variance (ANOVA) by Dunn's multiple comparison test was used. Differences were considered statistically significant at $P < 0.05$ (n.s., not significant). Diagnostic sensitivity and specificity, along with their 95% CIs, were calculated using the Clopper-Pearson exact method in MedCalc, whereas the means and SD for data distributions were derived from the sample using the corresponding functions in Excel.

Supplementary Materials

This PDF file includes:

Figs. S1 to S20
Tables S1 to S4
References

REFERENCES

1. J. C. M. Wan, C. Massie, J. Garcia-Corbacho, F. Mouliere, J. D. Brenton, C. Caldas, S. Pacey, R. Baird, N. Rosenfeld, Liquid biopsies come of age: Towards implementation of circulating tumour DNA. *Nat. Rev. Cancer* **17**, 223–238 (2017).
2. C. Alix-Panabières, K. Pantel, Liquid biopsy: From discovery to clinical application. *Cancer Discov.* **11**, 858–873 (2021).
3. R. Kalluri, V. S. LeBleu, The biology, function, and biomedical applications of exosomes. *Science* **367**, eaau6977 (2020).
4. J. Phallen, M. Sausen, V. Adleff, A. Leal, C. Hruban, J. White, V. Anagnostou, J. Fiksel, S. Cristiano, E. Papp, S. Speir, T. Reinert, M. W. Orntoft, B. D. Woodward, D. Murphy, S. Parpart-Li, D. Riley, M. Nesselbush, N. Sengamalay, A. Georgiadis, Q. K. Li, M. R. Madsen, F. V. Mortensen, J. Huiskens, C. Punt, N. van Grieken, R. Fijneman, G. Meijer, H. Husain, R. B. Scharpf, L. A. Diaz Jr., S. Jones, S. Angiuoli, T. Ørntoft, H. J. Nielsen, C. L. Andersen, V. E. Velculescu, Direct detection of early-stage cancers using circulating tumor DNA. *Sci. Transl. Med.* **9**, eaan2415 (2017).
5. P. Radfar, H. A. Es, R. Salomon, A. Kulasinghe, N. Ramalingam, E. Sarafraz-Yazdi, J. P. Thiery, M. E. Warkiani, Single-cell analysis of circulating tumour cells: Enabling technologies and clinical applications. *Trends Biotechnol.* **40**, 1041–1060 (2022).
6. E. Heitzer, I. S. Haque, C. E. S. Roberts, M. R. Speicher, Current and future perspectives of liquid biopsies in genomics-driven oncology. *Nat. Rev. Genet.* **20**, 71–88 (2019).
7. A. A. Chaudhuri, J. J. Chabon, A. F. Lovejoy, A. M. Newman, H. Stehr, T. D. Azad, M. S. Khodadoust, M. S. Esfahani, C. L. Liu, L. Zhou, F. Scherer, D. M. Kurtz, C. Say, J. N. Carter, D. J. Merriott, J. C. Dudley, M. S. Binkley, L. Modlin, S. K. Padda, M. F. Gensheimer, R. B. West, J. B. Shrager, J. W. Neal, H. A. Wakelee, B. W. Loo Jr., A. A. Alizadeh, M. Diehn, Early detection of molecular residual disease in localized lung cancer by circulating tumor DNA profiling. *Cancer Discov.* **7**, 1394–1403 (2017).
8. Y. M. D. Lo, D. S. C. Han, P. Jiang, R. W. K. Chiu, Epigenetics, fragmentomics, and topology of cell-free DNA in liquid biopsies. *Science* **372**, eaaw3616 (2021).
9. A. Tivey, M. Church, D. Rothwell, C. Dive, N. Cook, Circulating tumour DNA—Looking beyond the blood. *Nat. Rev. Clin. Oncol.* **19**, 600–612 (2022).
10. M. G. O. Fernandes, N. Cruz-Martins, J. C. Machado, J. L. Costa, V. Hespanhol, The value of cell-free circulating tumour DNA profiling in advanced non-small cell lung cancer (NSCLC) management. *Cancer Cell Int.* **21**, 675 (2021).
11. M. Murtaza, S. J. Dawson, D. W. Tsui, D. Gale, T. Forshew, A. M. Piskorz, C. Parkinson, S. F. Chin, Z. Kingsbury, A. S. Wong, F. Marass, S. Humphray, J. Hadfield, D. Bentley, T. M. Chin, J. D. Brenton, C. Caldas, N. Rosenfeld, Non-invasive analysis of acquired resistance to cancer therapy by sequencing of plasma DNA. *Nature* **497**, 108–112 (2013).
12. Y. Zhang, Y. Yao, Y. Xu, L. Li, Y. Gong, K. Zhang, M. Zhang, Y. Guan, L. Chang, X. Xia, L. Li, S. Jia, Q. Zeng, Pan-cancer circulating tumor DNA detection in over 10,000 Chinese patients. *Nat. Commun.* **12**, 11 (2021).
13. S. J. Dawson, D. W. Tsui, M. Murtaza, H. Biggs, O. M. Rueda, S. F. Chin, M. J. Dunning, D. Gale, T. Forshew, B. Mahler-Araujo, S. Rajan, S. Humphray, J. Becq, D. Halsall, M. Wallis, D. Bentley, C. Caldas, N. Rosenfeld, Analysis of circulating tumor DNA to monitor metastatic breast cancer. *N. Engl. J. Med.* **368**, 1199–1209 (2013).
14. C. Abbosh, N. J. Birkbak, G. A. Wilson, M. Jamal-Hanjani, T. Constantin, R. Salari, J. Le Quesne, D. A. Moore, S. Veeriah, R. Rosenthal, T. Marafioti, E. Kirkizlar, T. B. K. Watkins, N. McGranahan, S. Ward, L. Martinson, J. Riley, F. Fraioli, M. Al Bakir, E. Grönroos, F. Zambrana, R. Endozo, W. L. Bi, F. M. Fennessy, N. Sponer, D. Johnson, J. Laycock, S. Shafi, J. Czyzewska-Khan, A. Rowan, T. Chambers, N. Matthews, S. Turajlic, C. Hiley, S. M. Lee, M. D. Forster, T. Ahmad, M. Falzon, E. Borg, D. Lawrence, M. Hayward, S. Kolvekar, N. Panagiotopoulos, S. M. Janes, R. Thakrar, A. Ahmed, F. Blackhall, Y. Summers, D. Hafez, A. Naik, A. Ganguly, S. Kareht, R. Shah, L. Joseph, A. M. Quinn, P. A. Crosbie, B. Naidu, G. Middleton, G. Langman, S. Trotter, M. Nicolson, H. Remmen, K. Kerr, M. Chetty, L. Gomersall, D. A. Fennell, A. Nakas, S. Rathinam, G. Anand, S. Khan, P. Russell, V. Ezhil, B. Ismail, M. Irvin-Sellers, V. Prakash, J. F. Lester, M. Kornaszewska, R. Attanoos, H. Adams, H. Davies, D. Oukrif, A. U. Akarca, J. A. Hartley, H. L. Lowe, S. Lock, N. Iles, H. Bell, Y. Ngai, G. Elgar, Z. Szallasi, R. F. Schwarz, J. Herrero, A. Stewart, S. A. Quezada, K. S. Peggs, P. Van Loo, C. Dive, C. J. Lin, M. Rabinowitz, H. Aerts, A. Hackshaw, J. A. Shaw, B. G. Zimmermann, C. Swanton, Phylogenetic ctDNA analysis depicts early-stage lung cancer evolution. *Nature* **545**, 446–451 (2017).
15. J. Tie, Y. Wang, C. Tomasetti, L. Li, S. Springer, I. Kinde, N. Silliman, M. Tacey, H. L. Wong, M. Christie, S. Kosmider, I. Skinner, R. Wong, M. Steel, B. Tran, J. Desai, I. Jones, A. Haydon, T. Hayes, T. J. Price, R. L. Strausberg, L. A. Diaz Jr., N. Papadopoulos, K. W. Kinzler, B. Vogelstein, P. Gibbs, Circulating tumor DNA analysis detects minimal residual disease and predicts recurrence in patients with stage II colon cancer. *Sci. Transl. Med.* **8**, 346ra392 (2016).
16. A. Zviran, R. C. Schulman, M. Shah, S. T. K. Hill, S. Deochand, C. C. Khamnei, D. Maloney, K. Patel, W. Liao, A. J. Widman, P. Wong, M. K. Callahan, G. Ha, S. Reed, D. Rotem, D. Frederick, T. Sharova, B. Miao, T. Kim, G. Gydush, J. Rhoades, K. Y. Huang, N. D. Omans, P. O. Bolan, A. H. Lipsky, C. Ang, M. Malbari, C. F. Spinelli, S. Kazancioglu, A. M. Runnels, S. Fennessey, C. Stolte, F. Gaiti, G. G. Inghirami, V. Adalsteinsson, B. Houck-Loomis, J. Ishii, J. D. Wolchok, G. Boland, N. Robine, N. K. Altorki, D. A. Landau, Genome-wide cell-free DNA mutational integration enables ultra-sensitive cancer monitoring. *Nat. Med.* **26**, 1114–1124 (2020).
17. A. M. Newman, S. V. Bratman, J. To, J. F. Wynne, N. C. Eclov, L. A. Modlin, C. L. Liu, J. W. Neal, H. A. Wakelee, R. E. Merritt, J. B. Shrager, B. W. Loo Jr., A. A. Alizadeh, M. Diehn, An ultrasensitive method for quantitating circulating tumor DNA with broad patient coverage. *Nat. Med.* **20**, 548–554 (2014).
18. J. C. M. Wan, K. Heider, D. Gale, S. Murphy, E. Fisher, F. Mouliere, A. Ruiz-Valdepenas, A. Santonja, J. Morris, D. Chandrananda, A. Marshall, A. B. Gill, P. Y. Chan, E. Barker, G. Young, W. N. Cooper, I. Hudecova, F. Marass, R. Mair, K. M. Brindle, G. D. Stewart, J. E. Abraham, C. Caldas, D. M. Rassl, R. C. Rintoul, C. Alifrangis, M. R. Middleton, F. A. Gallagher, C. Parkinson, A. Durrani, U. McDermott, C. G. Smith, C. Massie, P. G. Corrie, N. Rosenfeld, ctDNA monitoring using patient-specific sequencing and integration of variant reads. *Sci. Transl. Med.* **12**, eaaz8084 (2020).
19. B. R. McDonald, T. Contente-Cuomo, S. J. Sammut, A. Odenheimer-Bergman, B. Ernst, N. Perdigones, S. F. Chin, M. Farooq, R. Mejia, P. A. Cronin, K. S. Anderson, H. E. Kosiorek, D. W. Northfelt, A. E. McCullough, B. K. Patel, J. N. Weitzel, T. P. Slavin, C. Caldas, B. A. Pockaj, M. Murtaza, Personalized circulating tumor DNA analysis to detect residual disease after neoadjuvant therapy in breast cancer. *Sci. Transl. Med.* **11**, eaax7392 (2019).
20. L. R. Wu, S. X. Chen, Y. Wu, A. A. Patel, D. Y. Zhang, Multiplexed enrichment of rare DNA variants via sequence-selective and temperature-robust amplification. *Nat. Biomed. Eng.* **1**, 714–723 (2017).
21. F. von Wintzingerode, O. Landt, A. Ehrlich, U. B. Göbel, Peptide nucleic acid-mediated PCR clamping as a useful supplement in the determination of microbial diversity. *Appl. Environ. Microbiol.* **66**, 549–557 (2000).

Downloaded from https://www.science.org on May 23, 2026

22. J. Zhang, J. Li, J. B. Saucier, Y. Feng, Y. Jiang, J. Sinson, A. K. McCombs, E. S. Schmitt, S. Peacock, S. Chen, H. Dai, X. Ge, G. Wang, C. A. Shaw, H. Mei, A. Breman, F. Xia, Y. Yang, A. Purgason, A. Pourpak, Z. Chen, X. Wang, Y. Wang, S. Kulkarni, K. W. Choy, R. J. Wapner, I. B. Van den Veyver, A. Beaudet, S. Parmar, L. J. Wong, C. M. Eng, Non-invasive prenatal sequencing for multiple Mendelian monogenic disorders using circulating cell-free fetal DNA. *Nat. Med.* **25**, 439–447 (2019).
23. G. Gydush, E. Nguyen, J. H. Bae, T. Blewett, J. Rhoades, S. C. Reed, D. Shea, K. Xiong, R. Liu, F. Yu, K. W. Leong, A. D. Choudhury, D. G. Stover, S. M. Tolaney, I. E. Krop, J. Christopher Love, H. A. Parsons, G. Mike Makrigiorgos, T. R. Golub, V. A. Adalsteinsson, Massively parallel enrichment of low-frequency alleles enables duplex sequencing at low depth. *Nat Biomed. Eng.* **6**, 257–266 (2022).
24. A. M. Newman, A. F. Lovejoy, D. M. Klass, D. M. Kurtz, J. J. Chabon, F. Scherer, H. Stehr, C. L. Liu, S. V. Bratman, C. Say, L. Zhou, J. N. Carter, R. B. West, G. W. Sledge, J. B. Shrager, B. W. Loo Jr., J. W. Neal, H. A. Wakelee, M. Diehn, A. A. Alizadeh, Integrated digital error suppression for improved detection of circulating tumor DNA. *Nat. Biotechnol.* **34**, 547–555 (2016).
25. M. W. Schmitt, S. R. Kennedy, J. J. Salk, E. J. Fox, J. B. Hiatt, L. A. Loeb, Detection of ultra-rare mutations by next-generation sequencing. *Proc. Natl. Acad. Sci. U.S.A.* **109**, 14508–14513 (2012).
26. A. Aalipour, J. C. Dudley, S. M. Park, S. Murty, J. J. Chabon, E. A. Boyle, M. Diehn, S. S. Gambhir, Deactivated CRISPR associated protein 9 for minor-allele enrichment in cell-free DNA. *Clin. Chem.* **64**, 307–316 (2018).
27. B. Kim, Y. Kim, S. Shin, S. T. Lee, J. Y. Cho, K. A. Lee, Application of CRISPR/Cas9-based mutant enrichment technique to improve the clinical sensitivity of plasma EGFR testing in patients with non-small cell lung cancer. *Cancer Cell Int.* **22**, 82 (2022).
28. K. Murugan, A. S. Seetharam, A. J. Severin, D. G. Sashital, CRISPR-Cas12a has widespread off-target and dsDNA-nicking effects. *J. Biol. Chem.* **295**, 5538–5553 (2020).
29. Q. Liu, X. Guo, G. Xun, Z. Li, Y. Chong, L. Yang, H. Wang, F. Zhang, S. Luo, L. Cui, P. Zhao, X. Ye, H. Xu, H. Lu, X. Li, Z. Deng, K. Li, Y. Feng, Argonaute integrated single-tube PCR system enables supersensitive detection of rare mutations. *Nucleic Acids Res.* **49**, e75 (2021).
30. J. Song, J. W. Hegge, M. G. Mauk, J. Chen, J. E. Till, N. Bhagwat, L. T. Azink, J. Peng, M. Sen, J. Mays, E. L. Carpenter, J. van der Oost, H. H. Bau, Highly specific enrichment of rare nucleic acid fractions using *Thermus thermophilus* argonaute with applications in cancer diagnostics. *Nucleic Acids Res.* **48**, e19 (2020).
31. S. R. Rananaware, E. K. Vesco, G. M. Shoemaker, S. S. Anekar, L. S. W. Sandoval, K. S. Meister, N. C. Macaluso, L. T. Nguyen, P. K. Jain, Programmable RNA detection with CRISPR-Cas12a. *Nat. Commun.* **14**, 5409 (2023).
32. M. Lin, H. Yue, T. Tian, E. Xiong, D. Zhu, Y. Jiang, X. Zhou, Glycerol additive boosts 100-fold sensitivity enhancement for one-pot RPA-CRISPR/Cas12a assay. *Anal. Chem.* **94**, 8277–8284 (2022).
33. F. Diehl, M. Li, D. Dressman, Y. He, D. Shen, S. Szabo, L. A. Diaz Jr., S. N. Goodman, K. A. David, H. Juhl, K. W. Kinzler, B. Vogelstein, Detection and quantification of mutations in the plasma of patients with colorectal tumors. *Proc. Natl. Acad. Sci. U.S.A.* **102**, 16368–16373 (2005).
34. N. M. Kuderer, K. A. Burton, S. Blau, A. L. Rose, S. Parker, G. H. Lyman, C. A. Blau, Comparison of 2 commercially available next-generation sequencing platforms in oncology. *JAMA Oncol.* **3**, 996–998 (2017).
35. L. A. Diaz Jr., A. Bardelli, Liquid biopsies: Genotyping circulating tumor DNA. *J. Clin. Oncol.* **32**, 579–586 (2014).
36. P. Jiang, Y. M. D. Lo, The long and short of circulating cell-free DNA and the ins and outs of molecular diagnostics. *Trends Genet.* **32**, 360–371 (2016).
37. M. W. Snyder, M. Kircher, A. J. Hill, R. M. Daza, J. Shendure, Cell-free DNA comprises an in vivo nucleosome footprint that informs its tissues-of-origin. *Cell* **164**, 57–68 (2016).
38. P. Jiang, C. W. Chan, K. C. Chan, S. H. Cheng, J. Wong, V. W. Wong, G. L. Wong, S. L. Chan, T. S. Mok, H. L. Chan, P. B. Lai, R. W. Chiu, Y. M. Lo, Lengthening and shortening of plasma DNA in hepatocellular carcinoma patients. *Proc. Natl. Acad. Sci. U.S.A.* **112**, E1317–E1325 (2015).
39. H. R. Underhill, J. O. Kitzman, S. Hellwig, N. C. Welker, R. Daza, D. N. Baker, K. M. Gligorich, R. C. Rostomily, M. P. Bronner, J. Shendure, Fragment length of circulating tumor DNA. *PLOS Genet.* **12**, e1006162 (2016).
40. C. Sanchez, M. W. Snyder, R. Tanos, J. Shendure, A. R. Thierry, New insights into structural features and optimal detection of circulating tumor DNA determined by single-strand DNA analysis. *NPJ Genom. Med.* **3**, 31 (2018).
41. J. van de Haar, X. Ma, S. N. Ooft, P. W. van der Helm, L. R. Hoes, S. Mainardi, D. J. Pinato, K. Sun, L. Salvatore, G. Tortora, I. V. Zurlo, S. Leo, R. Giampieri, R. Berardi, F. Gelsomino, V. Merz, F. Mazzuca, L. Antonuzzo, G. Rosati, C. Stavraka, P. Ross, M. G. Rodriquenz, M. Pavarana, C. Messina, T. Iveson, F. Zoratto, A. Thomas, E. Fenocchio, M. Ratti, I. Depetris, M. Cergnul, C. Morelli, M. Libertini, A. Parisi, M. De Tursi, N. Zanaletti, O. Garrone, J. Graham, R. Longarini, S. M. Gobba, A. Petrillo, E. Tamburini, N. La Verde, F. Petrelli, V. Ricci, L. F. A. Wessels, M. Ghidini, A. Cortellini, E. E. Voest, N. Valeri, Codon-specific KRAS mutations predict survival benefit of trifluridine/tipiracil in metastatic colorectal cancer. *Nat. Med.* **29**, 605–614 (2023).
42. P. East, G. P. Kelly, D. Biswas, M. Marani, D. C. Hancock, T. Creasy, K. Sachsenmeier, C. Swanton, J. Downward, S. de Carné Trécesson, RAS oncogenic activity predicts response to chemotherapy and outcome in lung adenocarcinoma. *Nat. Commun.* **13**, 5632 (2022).
43. A. M. Varghese, M. A. Perry, J. F. Chou, S. Nandakumar, D. Muldoon, A. Erakky, A. Zucker, C. Fong, M. Mehine, B. Nguyen, O. Basturk, F. Balogun, D. P. Kelsen, A. R. Brannon, D. Mandelker, E. Vakiani, W. Park, K. H. Yu, Z. K. Stadler, M. A. Schattner, W. R. Jarnagin, A. C. Wei, D. Chakravarty, M. Capanu, N. Schultz, M. F. Berger, C. A. Iacobuzio-Donahue, C. Bandlamudi, E. M. O'Reilly, Clinicogenomic landscape of pancreatic adenocarcinoma identifies KRAS mutant dosage as prognostic of overall survival. *Nat. Med.* **31**, 466–477 (2025).
44. A. Bulle, P. Liu, K. Seehra, S. Bansod, Y. Chen, K. Zahra, V. Somani, I. A. Khawar, H. P. Chen, P. B. Dodhiawala, L. Li, Y. Geng, C. K. Mo, J. Mahsl, L. Ding, R. Govindan, S. Davies, J. Mudd, W. G. Hawkins, R. C. Fields, D. G. DeNardo, D. Knoerzer, J. M. Held, P. M. Grierson, A. Wang-Gillam, M. B. Ruzinova, K. H. Lim, Combined KRAS-MAPK pathway inhibitors and HER2-directed drug conjugate is efficacious in pancreatic cancer. *Nat. Commun.* **15**, 2503 (2024).
45. S. Eser, N. Reiff, M. Messer, B. Seidler, K. Gottschalk, M. Dobler, M. Hieber, A. Arbeiter, S. Klein, B. Kong, C. W. Michalski, A. M. Schlitter, I. Esposito, A. J. Kind, L. Rad, A. E. Schnieke, M. Baccarini, D. R. Alessi, R. Rad, R. M. Schmid, G. Schneider, D. Saur, Selective requirement of PI3K/PDK1 signaling for Kras oncogene-driven pancreatic cell plasticity and cancer. *Cancer Cell* **23**, 406–420 (2013).
46. S. Misale, R. Yaeger, S. Hobor, E. Scala, M. Janakiraman, D. Liska, E. Valtorta, R. Schiavo, M. Buscarino, G. Siravegna, K. Bencardino, A. Cercek, C. T. Chen, S. Veronese, C. Zanon, A. Sartore-Bianchi, M. Gambacorta, M. Gallicchio, E. Vakiani, V. Boscaro, E. Medico, M. Weiser, S. Siena, F. Di Nicolantonio, D. Solit, A. Bardelli, Emergence of KRAS mutations and acquired resistance to anti-EGFR therapy in colorectal cancer. *Nature* **486**, 532–536 (2012).
47. G. Improta, A. Zupa, L. Possidente, A. Tartarone, P. Pedicini, A. Nappi, S. Molinari, F. Fraggetta, G. Vita, Coexistence of two different mutations in codon 12 of the Kras gene in colorectal cancer: Report of a case supporting the concept of tumoral heterogeneity. *Oncol. Lett.* **5**, 1741–1743 (2013).
48. J. Hallin, V. Bowcut, A. Calinisan, D. M. Briere, L. Hargis, L. D. Engstrom, J. Laguer, J. Medwid, D. Vanderpool, E. Lifset, D. Trinh, N. Hoffman, X. Wang, J. David Lawson, R. J. Gunn, C. R. Smith, N. C. Thomas, M. Martinson, A. Bergstrom, F. Sullivan, K. Bouhana, S. Winski, L. He, J. Fernandez-Banet, A. Pavlicek, J. R. Haling, L. Rahbaek, M. A. Marx, P. Olson, J. G. Christensen, Anti-tumor efficacy of a potent and selective non-covalent KRAS(G12D) inhibitor. *Nat. Med.* **28**, 2171–2182 (2022).
49. D. Wei, L. Wang, X. Zuo, A. Maitra, R. S. Bresalier, A small molecule with big impact: MRTX1133 targets the KRASG12D mutation in pancreatic cancer. *Clin. Cancer Res.* **30**, 655–662 (2024).
50. "A phase 1/2 multiple expansion cohort trial of MRTX1133 in patients with advanced solid tumors harboring a KRAS G12D mutation" (US National Library of Medicine, 2023); https://clinicaltrials.gov/study/NCT05737706?intr=MRTX1133.
51. C. S. Karapetis, S. Khambata-Ford, D. J. Jonker, C. J. O'Callaghan, D. Tu, N. C. Tebbutt, R. J. Simes, H. Chalchal, J. D. Shapiro, S. Robitaille, T. J. Price, L. Shepherd, H. J. Au, C. Langer, M. J. Moore, J. R. Zalcberg, K-ras mutations and benefit from cetuximab in advanced colorectal cancer. *N. Engl. J. Med.* **359**, 1757–1765 (2008).
52. V. Thoeny, E. Melnik, M. Huetter, M. Asadi, P. Mehrabi, T. Schalkhammer, W. Pulverer, T. Maier, G. C. Mutinati, P. Lieberzeit, R. Hainberger, Recombinase polymerase amplification in combination with electrochemical readout for sensitive and specific detection of PIK3CA point mutations. *Anal. Chim. Acta* **1281**, 341922 (2023).
53. K. A. V. Kohabir, L. O. Nooi, A. Brink, R. H. Brakenhoff, E. A. Sistermans, R. M. F. Wolthuis, In vitro CRISPR-Cas12a-based detection of cancer-associated TP53 hotspot mutations beyond the crRNA seed region. *Crispr j* **6**, 127–139 (2023).
54. A. Deng, Z. Mao, X. Jin, W. Lv, L. Huang, H. Zhong, S. Wang, Y. Shi, T. Zhou, J. Zhao, Q. Huang, X. Luo, L. Ma, H. Zou, R. Fu, G. Huang, ID-CRISPR: A CRISPR/Cas12a platform for label-free and sensitive detection of rare mutant alleles using self-interference DNA hydrogel reporter. *Biosens. Bioelectron.* **278**, 117309 (2025).
55. H. A. Parsons, T. Blewett, X. Chu, S. Sridhar, K. Santos, K. Xiong, V. G. Abramson, A. Patel, J. Cheng, A. Brufsky, J. Rhoades, J. Force, R. Liu, T. A. Traina, L. A. Carey, M. F. Rimawi, K. D. Miller, V. Stearns, J. Specht, C. Falkson, H. J. Burstein, A. C. Wolff, E. P. Winer, N. Tayob, I. E. Krop, G. M. Makrigiorgos, T. R. Golub, E. L. Mayer, V. A. Adalsteinsson, Circulating tumor DNA association with residual cancer burden after neoadjuvant chemotherapy in triple-negative breast cancer in TBCRC 030. *Ann. Oncol.* **34**, 899–906 (2023).
56. E. J. Moding, B. Y. Nabet, A. A. Alizadeh, M. Diehn, Detecting liquid remnants of solid tumors: Circulating tumor DNA minimal residual disease. *Cancer Discov.* **11**, 2968–2986 (2021).
57. A. R. Parikh, E. E. Van Seventer, G. Siravegna, A. V. Hartwig, A. Jaimovich, Y. He, K. Kanter, M. G. Fish, K. D. Fosbenner, B. Miao, S. Phillips, J. H. Carmichael, N. Sharma, J. Jarnagin, I. Baiev, Y. S. Shah, I. J. Fetter, H. A. Shahzade, J. N. Allen, L. S. Blaszkowsky, J. W. Clark, J. S. Dubois, J. W. Franses, B. J. Giantonio, L. Goyal, S. J. Klempner, R. D. Nipp, E. J. Roeland,

Downloaded from https://www.science.org on May 23, 2026

D. P. Ryan, C. D. Weekes, J. Y. Wo, T. S. Hong, L. Bordeianou, C. R. Ferrone, M. Qadan, H. Kunitake, D. Berger, R. Ricciardi, J. C. Cusack, V. M. Raymond, A. Talasaz, G. M. Boland, R. B. Corcoran, Minimal residual disease detection using a plasma-only circulating tumor DNA assay in patients with colorectal cancer. *Clin. Cancer Res.* **27**, 5586–5594 (2021).
58. M. Ignatiadis, G. W. Sledge, S. S. Jeffrey, Liquid biopsy enters the clinic—Implementation issues and future challenges. *Nat. Rev. Clin. Oncol.* **18**, 297–312 (2021).
59. D. M. Kurtz, J. Soo, L. C. T. Keh, S. Alig, J. J. Chabon, B. J. Sworder, A. Schultz, M. C. Jin, F. Scherer, A. Garofalo, C. W. Macaulay, E. G. Hamilton, B. Chen, M. Olsen, J. G. Schroers-Martin, A. F. M. Craig, E. J. Moding, M. S. Esfahani, C. L. Liu, U. Dührsen, A. Hüttmann, R. O. Casasnovas, J. R. Westin, M. Roschewski, W. H. Wilson, G. Gaidano, D. Rossi, M. Diehn, A. A. Alizadeh, Enhanced detection of minimal residual disease by targeted sequencing of phased variants in circulating tumor DNA. *Nat. Biotechnol.* **39**, 1537–1547 (2021).
60. "A phase 1 trial evaluating the safety, tolerability, PK, and efficacy of QTX3034 in patients with solid tumors with KRASG12D mutation" (US National Library of Medicine, 2025); https://clinicaltrials.gov/study/NCT06227377.
61. "An open-label, single-center, single-arm phase IIa study to evaluate the safety and efficacy of vebreltinib in combination with osimertinib in patients with locally advanced or metastatic non-small cell lung cancer with EGFR 21 L858R mutation" (L. Avistone Biotechnology Co., Ed., 2025); https://clinicaltrials.gov/study/NCT06827145.
62. A. Marusyk, M. Janiszewska, K. Polyak, Intratumor heterogeneity: The Rosetta Stone of therapy resistance. *Cancer Cell* **37**, 471–484 (2020).
63. J. Song, M. H. Cho, H. Cho, Y. Song, S. W. Lee, H. C. Nam, T. H. Yoon, J. C. Shin, J. S. Hong, Y. Kim, E. Ekanayake, J. Jeon, D. G. You, S. G. Im, G. S. Choi, J. S. Park, B. C. Carter, L. Balaj, A. N. Seo, M. A. Miller, S. Y. Park, T. Kang, C. M. Castro, H. Lee, Amplifying mutational profiling of extracellular vesicle mRNA with SCOPE. *Nat. Biotechnol.* **43**, 1485–1495 (2025).
64. A. R. Thierry, Circulating DNA fragmentomics and cancer screening. *Cell Genom.* **3**, 100242 (2023).
65. S. R. Greytak, K. B. Engel, S. Parpart-Li, M. Murtaza, A. J. Bronkhorst, M. D. Pertile, H. M. Moore, Harmonizing cell-free DNA collection and processing practices through evidence-based guidance. *Clin. Cancer Res.* **26**, 3104–3109 (2020).
66. C. M. Lockwood, L. Borsu, M. Cankovic, J. S. L. Earle, C. D. Gocke, M. Hameed, D. Jordan, J. R. Lopategui, M. Pullambhatla, J. Reuther, K. M. Rumilla, L. J. Tafe, R. L. Temple-Smolkin, P. Terraf, A. M. Tsimberidou, Recommendations for cell-free DNA assay validations: A joint consensus recommendation of the Association for Molecular Pathology and College of American Pathologists. *J. Mol. Diagn.* **25**, 876–897 (2023).
67. V. D. de Jager, P. Giacomini, J. A. Fairley, R. A. Toledo, S. J. Patton, S. A. Joosse, C. Koch, Z. C. Deans, K. Pantel, E. Heitzer, E. Schuuring, Reporting of molecular test results from cell-free DNA analyses: Expert consensus recommendations from the 2023 European Liquid Biopsy Society ctDNA Workshop. *EBioMedicine* **114**, 105636 (2025).
68. B. J. Hindson, K. D. Ness, D. A. Masquelier, P. Belgrader, N. J. Heredia, A. J. Makarewicz, I. J. Bright, M. Y. Lucero, A. L. Hiddessen, T. C. Legler, T. K. Kitano, M. R. Hodel, J. F. Petersen, P. W. Wyatt, E. R. Steenblock, P. H. Shah, L. J. Bousse, C. B. Troup, J. C. Mellen, D. K. Wittmann, N. G. Erndt, T. H. Cauley, R. T. Koehler, A. P. So, S. Dube, K. A. Rose, L. Montesclaros, S. Wang, D. P. Stumbo, S. P. Hodges, S. Romine, F. P. Milanovich, H. E. White, J. F. Regan, G. A. Karlin-Neumann, C. M. Hindson, S. Saxonov, B. W. Colston, High-throughput droplet digital PCR system for absolute quantitation of DNA copy number. *Anal. Chem.* **83**, 8604–8610 (2011).
69. L. B. Pinheiro, V. A. Coleman, C. M. Hindson, J. Herrmann, B. J. Hindson, S. Bhat, K. R. Emslie, Evaluation of a droplet digital polymerase chain reaction format for DNA copy number quantification. *Anal. Chem.* **84**, 1003–1011 (2012).
70. J. S. Chen, E. Ma, L. B. Harrington, M. Da Costa, X. Tian, J. M. Palefsky, J. A. Doudna, CRISPR-Cas12a target binding unleashes indiscriminate single-stranded DNase activity. *Science* **360**, 436–439 (2018).
71. C. Myhrvold, C. A. Freije, J. S. Gootenberg, O. O. Abudayyeh, H. C. Metsky, A. F. Durbin, M. J. Kellner, A. L. Tan, L. M. Paul, L. A. Parham, K. F. Garcia, K. G. Barnes, B. Chak, A. Mondini, M. L. Nogueira, S. Isern, S. F. Michael, I. Lorenzana, N. L. Yozwiak, B. L. MacInnis, I. Bosch, L. Gehrke, F. Zhang, P. C. Sabeti, Field-deployable viral diagnostics using CRISPR-Cas13. *Science* **360**, 444–448 (2018).

Acknowledgments: Figures were created using BioRender.com. **Funding:** This work was partially supported by National Institutes of Health grant U01CA269147 (to C.L.)., National Institutes of Health grant U01AI148306 (to C.L.)., and UConn Research Excellence Program award (to C.L.). **Author contributions:** Conceptualization: C.G., S.Z., R.Ye., J.Z., X.G., R.Ya., R.A.C., and C.L. Methodology: C.G., S.Z., R.Ye., J.Z., R.Ya., C.H., Z.L., and C.L. Software: C.G., S.Z., R.Ye., J.Z., and R.Y. Validation: C.G., S.Z., R.Ye., J.Z., R.Ya., C.H., M.P., K.T.S., X.L., Z.L., and O.I. Formal analysis: C.G., W.G., and C.L. Investigation: C.G., S.Z., R.Ye., J.Z., and R.Ya. Resources: L.P. and C.L. Data curation: C.G., S.Z., and C.L. Writing—original draft: C.G., S.Z., J.Z., C.H., K.T.S., and R.A.C. Writing—review and editing: C.G., S.Z., R.Ye., J.Z., X.G., R.Ya., C.H., M.P., X.L., Z.L., L.P., W.G., O.I., and C.L. Visualization: C.G. and C.L. Supervision: C.L. Project administration: C.L. Funding acquisition: C.L. **Competing interests:** C.G. and C.L. are inventors on a patent application (pending) submitted by University of Connecticut, which covers SNV detection reported in this study. The other authors declare that they have no competing interests. **Data, code, and materials availability** All data and code needed to evaluate and reproduce the conclusions in the paper are present in the paper and/or the Supplementary Materials. The code used in this study is available at https://doi.org/10.5281/zenodo.18883677 and https://doi.org/10.5281/zenodo.18883654. No new materials were generated in this study. All materials used in this research are commercially available, and their sources are described in Materials and Methods.

Submitted 17 October 2025
Accepted 20 April 2026
Published 22 May 2026
10.1126/sciadv.aed1757

Downloaded from https://www.science.org on May 23, 2026

ScienceAdvances

Single-nucleotide variant profiling in liquid biopsy with RECO-Cas

Chong Guo, Shuo Zhang, Ramachandra Yerramsetti, Jiongyu Zhang, Xin Guan, Rui Yang, Chengyu Hou, Minjie Pei, Kurt T. Schalper, Xingye Liu, Ziyue Li, Lorrie Perpetua, Wenqi Gan, Omar Ibrahim, Rachael A. Clark, and Changchun Liu

Sci. Adv. **12** (21), eaed1757. DOI: 10.1126/sciadv.aed1757

View the article online
https://www.science.org/doi/10.1126/sciadv.aed1757
Permissions
https://www.science.org/help/reprints-and-permissions

Downloaded from https://www.science.org on May 23, 2026

Use of this article is subject to the Terms of service

Science Advances (ISSN 2375-2548) is published by the American Association for the Advancement of Science. 1200 New York Avenue NW, Washington, DC 20005. The title *Science Advances* is a registered trademark of AAAS.

Copyright © 2026 The Authors, some rights reserved; exclusive licensee American Association for the Advancement of Science. No claim to original U.S. Government Works. Distributed under a Creative Commons Attribution NonCommercial License 4.0 (CC BY-NC).